**Evaluation of Subsurface Gypsum-rich Rock in the Context of Geologic Carbon Sequestration**

by

Jamie Rene Newsome

A thesis submitted to the Graduate Faculty of
Auburn University
in partial fulfillment of the
requirements for the Degree of
Master of Science

Auburn, Alabama
December 9, 2023

Keywords: Reactive transport modeling, gypsum, carbon storage, batch experiment, $CO_2$-brine-mineral reaction



Approved by

Lauren E. Beckingham, Chair, W. Allen and Martha Reed Endowed Associate Professor of Civil and Environmental Engineering
Mark Barnett, Professor of Civil and Environmental Engineering
Joel Hayworth, Elton Z. and Lois G. Huff Associate Professor of Civil and Environmental Engineering

## Abstract

Geological carbon sequestration is a promising means of reducing atmospheric carbon dioxide emissions by capturing $CO_2$ gas and storing it long term in subsurface porous rock. The goal of geologic carbon sequestration is to sequester $CO_2$ in an aqueous, solid, or gaseous form so it cannot re-enter the atmosphere. In this study, a gypsum-rich rock sample from Cassville, Georgia was analyzed as a potential injection site for carbon sequestration. Before injection, it is of the utmost importance to have an accurate prediction of the geochemical processes that will occur with the addition of $CO_2$ to the formation. The specific reactions studied include the initial acidification of the brine present in this sample and the mineral dissolution and precipitation reactions between $CO_2$ and gypsum, dolomite, quartz, and illite (the minerals present in this sample). These dissolution reactions are highly dynamic, and the goal of the models is to provide an accurate prediction of the rate, extent, and impact of the geochemical reactions on the formation. The reactive transport modeling software Crunchflow was used to model these dynamic processes. Images of the sample were taken using a scanning electron microscope (SEM) with a backscatter electron (BSE) detector. These images were used to calculate the porosity of the sample. This data was used to inform the reactive transport model. The results of this model provide predictions of changes in this formation including porosity, mineral dissolution, and potential mineral precipitation. The results from this model suggest that gypsum will remain stable in these conditions. The simulation results also show that dolomite will dissolve completely triggering an increase in porosity from 26% to 33%. In addition to modeling, this study also includes batch reactor experiments to validate the stability of gypsum in $CO_2$ storage conditions. Two sets of experiments are carried out exposing samples to conditions pertinent for storage formations: one

for pure gypsum, and one for Sample 9 from the Cassville, GA site. The concentration of calcium ions in the effluent solution was used as an indicator of the amount of gypsum dissolved. SEM imaging was utilized to note the morphological differences in the sample pre and post experiment.

## Acknowledgments

This project is supported by the Southeast Regional $CO_2$ Utilization and Storage Partnership (SECARB-USA), funded by the U.S. Department of Energy grant DE-FE0031830

I am overwhelmingly grateful to have had the opportunity to work under Dr. Lauren Beckingham in this program. Lauren has truly gone above and beyond her requirements as a research advisor and without her, my experience in this program would have looked drastically different. I am honored to have learned from her expertise and experience in research and engineering. Lauren's mentorship as a fellow woman in engineering has been and will continue to be invaluable to me.

I would also like to thank my family for their support throughout the duration of this program. To my parents, thank you for the calming phone calls, the respite weekends spent back home, and always reminding me to stay focused. You both have been so encouraging and reassuring to me throughout my academic career. To my siblings, thank you for always reminding me things are going to work out and of your unwavering faith in my abilities.

The contributions of my fellow WRISES group members do not go unnoticed. I would like to extend a sincere thank you to all you who have helped me along the way. Nora, Fahim, Nahian, Otis, Mitra, Parisa, Zhoufan, Driba, and Mohammad, it has been an honor to work as your peers and I am grateful for your assistance.

## List of Tables

## List of Abbreviations

| | |
|---|---|
| SEM | Scanning electron microscope |
| BSE | Backscatter electron |
| EOR | Enhanced oil recovery |
| RTM | Reactive transport model |
| GCS | Geologic carbon sequestration |
| XRD | X-ray diffraction |
| BET | Brunauer-Emmett-Teller |
| IC | Ion Chromatography |
| EDS | Element dispersive spectroscopy |

## List of Figures

## Table of Contents

# Chapter 1. Introduction

## 1.1 Background

Carbon dioxide ($CO_2$) is widely regarded by environmental agencies and researchers to be the greenhouse gas of primary concern due to its global ubiquity and abundance. The concentration of $CO_2$ in the atmosphere has increased by more than 40% since 1800 with over half the increase occurring since the mid-1970s when global energy consumption skyrocketed. (NAS, 2020). Much of this increase is due to anthropogenic activities, namely the burning of fossil fuels. The extraction of fossil fuels to burn for energy has disrupted the natural carbon cycle and increased atmospheric concentrations of $CO_2$.

This increase in emissions of $CO_2$ has had noted impacts on climate. The rate of global sea level rise has more than doubled in the past ten years compared to the majority of the twentieth century (NOAA, 2022). Studies conducted by the United Nations Environment Program suggest that the worldwide risk of wildfires could increase up to 57% in some areas (UNEP, 2022). In the United States alone, the annual average temperature is projected to increase by 2.5°F in the following three decades (Vose, R. et al, 2017). There is strong public, commercial, and governmental interest in stabilizing the rate of $CO_2$ emissions to mitigate the effects of climate change.

## 1.2 Geologic Carbon Sequestration

Carbon sequestration, simply put, is the capture, removal, and storage of $CO_2$ from the atmosphere. It occurs most often in the environment naturally through biological carbon sequestration in forests, soils, oceans, and ice (Lal, 2008). However, there is motivation to utilize engineered carbon sequestration methods to mitigate the large increase in $CO_2$ emissions from

anthropogenic sources. The goal of engineered carbon sequestration is to secure and stabilize $CO_2$ so it cannot re-enter the atmosphere. In geologic carbon sequestration (GCS), this is accomplished by injecting $CO_2$ into subsurface porous rock for long term storage. The temperature and pressure of the reservoir determine what state the $CO_2$ will be stored as. $CO_2$ enters its supercritical state when it is subjected to pressure greater than 7.38 MPa and temperatures greater than 31.1°C. At the supercritical point all three phases exist, passed this $CO_2$ is in its supercritical state (Fig. 1).

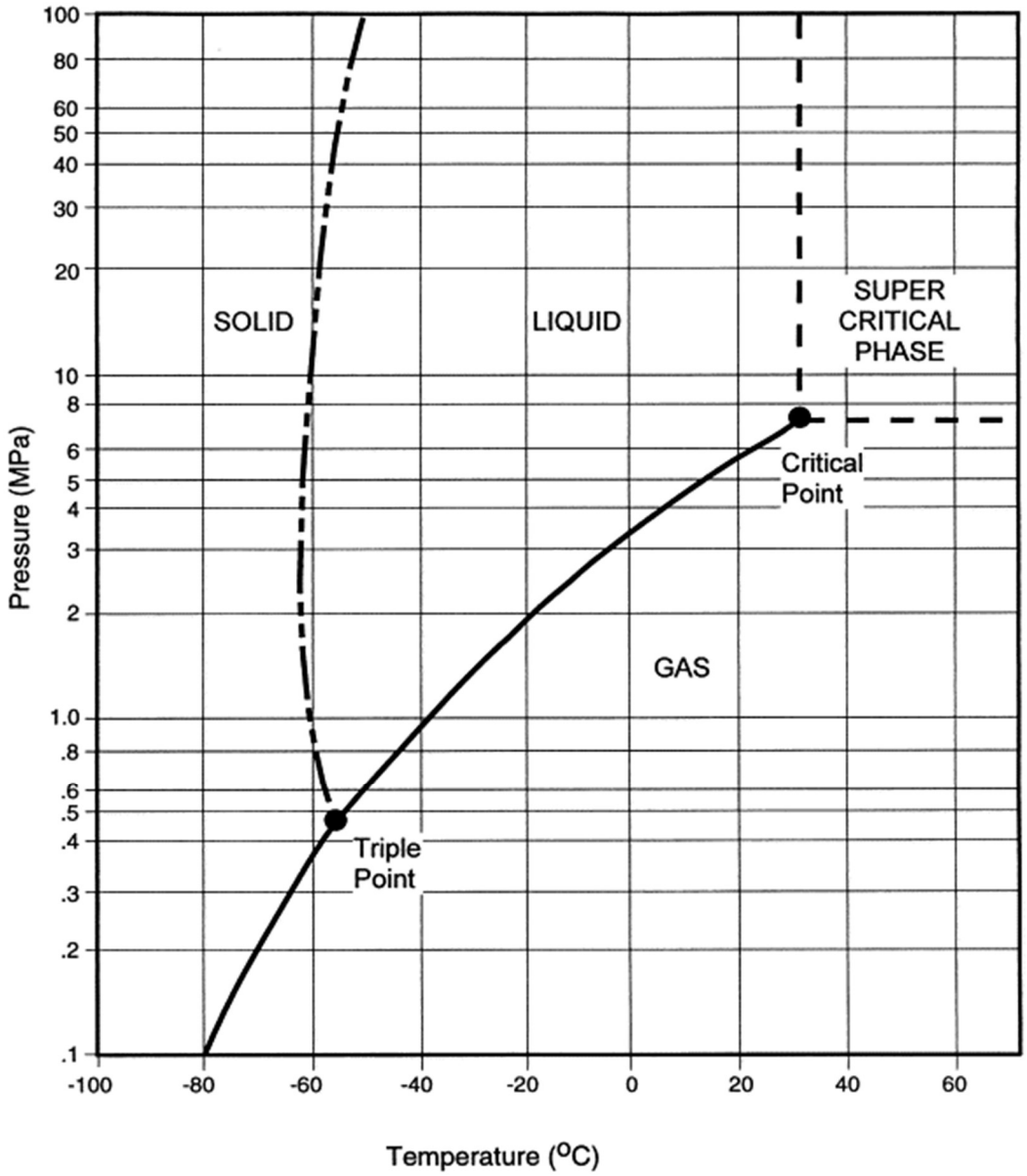


*Figure 1. Carbon dioxide phase diagram (Bachu, 2000).*

When carbon dioxide is in the supercritical state, it behaves like a super compressed gas, but with density increased to a liquid-like level, from 200 to 900 kg/m$^3$, approaching the density of water (Bachu, 2000). In deep saline aquifers, such as the potential injection sites evaluated in this work, $CO_2$ is subjected to these conditions. Deep saline aquifers are considered favorable for GCS due to their large potential storage space in porous media and the fact that the saline water is not useful for other agricultural or industrial purposes (Dai et al, 2020). As $CO_2$ is added to the aquifer, it dissolves and reacts with the brine to form carbonic acid, bicarbonate, and carbonate. These reactions are depicted below in Equations 1, 2, 3, and 4 respectively.

$$CO_2(g) \leftrightarrow CO_2(aq) \tag{1}$$

$$H_2O + CO_2\,(aq) \leftrightarrow H_2CO_3 \tag{2}$$

$$H_2CO_3 \leftrightarrow H^+ + HCO_3^- \tag{3}$$

$$HCO_3^- \leftrightarrow H^+ + CO_3^{2-} \tag{4}$$

As the reactions occur, conditions become increasingly acidic. In some formations in which calcium is present, carbonate can react with the calcium in solution to trigger calcite precipitation. This reaction is depicted in the following Equation 5.

$$Ca^{2+} + CO_3^{2-} \leftrightarrow CaCO_3(s) \tag{5}$$

In this reaction, the injected $CO_2$ is transformed into a solid mineral phase, calcite or aragonite here, and is considered permanently sequestered and will never re-enter the atmosphere. However, Equation 5 is a dynamic process and the direction it occurs (i.e “forwards” being precipitation, “backwards” being dissolution) depends heavily on the pH and ion concentrations in solution of the system.

Additional motivation behind geologic carbon sequestration specifically lies in gas injection enhanced oil recovery (EOR). Injected natural gases like $CO_2$ are miscible with oil and can thus mobilize otherwise immobile oil in depleted oil reservoirs. $CO_2$ is most commonly used for EOR since it also decreases the viscosity of oil. EOR has large economic motivations for fossil fuel companies as it can produce 30%-60% of a depleted oil reservoir's original oil content (DOE, 2022).

### 1.3 Reactive Transport Modeling in Crunchflow

Reactive transport models (RTMs) have been utilized to better understand biogeochemical systems for decades (Dai et al., 2020; Qin and Beckingham, 2021; Steefel et al., 2005, 2013). What distinguishes RTMs from other geochemical models is the coupling of flow and transport within a full geochemical thermodynamic and kinetic framework (Li et al 2017, Steefel et al., 2015). RTMs can simulate a broad range of processes including fluid flow of singular or multiple phases; solute transport via advection, dispersion, or diffusion; geochemical reactions such as mineral dissolution and precipitation, ion exchange, and surface complexation; and biogeochemical processes such as microbe-mediated redox reactions and biomass growth and decay (Li et al., 2017). This broad range of processes translates to a wide range of applications, making RTMs useful in simulating chemical weathering, soil formation, bioremediation, nuclear waste disposal, and carbon sequestration. Crunchflow is a reactive transport simulation software developed by Carl I. Steefel in the 1990s that will be utilized in this work (Steefel and Lasaga. 1994).

RTMs most often solve conservation of mass, momentum, and energy conservation equations (Steefel et al., 2005). Crunchflow specifically first partitions aqueous species into primary and secondary classes. The primary species are consider the foundations of the chemical systems of interest upon which the secondary species' concentrations are written through laws of

thermodynamics (Li ). The following is the reactive transport equation used in Crunchflow for a primary species (i) in the aqueous phase:

$$\frac{\partial(\Phi C_i)}{\partial t} + \nabla \cdot (-D\nabla C_i) + \nabla \cdot (uC_i) + R_i = 0 \quad (6)$$

where $C_i$ = total concentration of species $i$ (mol)

$t$ = time (seconds)

$D$ = combined dispersion-diffusion tensor ($m^2/s$)

$u$ = Darcy flow velocity vector (m/s)

$R_i$ = reaction rate of species $i$ ($mol/L^3 \cdot s$)

Equation 6 can be separated into four terms in units of moles of species $i$ per cubic liter of porous media · time. The first term represents the mass accumulation rate of the species that changes depending on chemical and physical processes; the second term accounts for the dispersion and diffusion processes, the third term accounts for the advection processes, and the last term of the equation accounts for the reactions. Note that the species may be involved in several reactions, in which case the fourth term would become a summation of all reaction rates. This equation presents the basic framework of the Crunchflow code.

In this study, Crunchflow reactive transport modeling will be utilized to consider $CO_2$ storage in a potential injection well located in Cassville, Georgia. Specifically, the gypsum-rich sample from the otherwise dolostone well will be the focus of inquiry. The goal of these models is to quantify and predict the geochemical processes that could occur if $CO_2$ were injected to this well including porosity evolution, mineral dissolution and precipitation, and ion concentrations.

### 1.4 Cassville, GA Site Details

The site analyzed this study is located in Cassville, an unincorporated community in Bartow County, Georgia. All samples were collected from the Cassville stratigraphic test well. Cassville is in the northwest region of Georgia, approximately 55 miles north of Atlanta. The approximate site location is depicted below in Figure 2.


*Figure 2. Location of Cassville, GA well (USGS)*

A total depth of 6,030 feet was reached in the creation of this well and open-hole geophysical data, formation microimager data, and side-wall core data were collected. The test well facility can be observed in Figure 3.

*Figure 3. Aerial photograph of Cassville stratigraphic test well located in Bartow County, Georgia (SSEB)*

Bartow County is in two geometric provinces, Paleozoic and Piedmont. The Cassville well is located in the Paleozoic province which consists of limestone, dolomite, sandstone, and shale (Croft, 1963). The majority of the Cassville well samples are dolomite, with one gypsum sample and one sandstone sample. This work is focused on the gypsum sample, Sample 9, taken from a depth of 3866.97 feet.

### 1.5 Reactive transport modeling of subsurface gypsum-rich in the context of geologic carbon sequestration

Many studies have explored the carbonation of gypsum ($CaSO_4 \cdot 2H_2O$) as a means of ex-situ carbon sequestration (Seo et al, 2018; Rahmani, 2018; Lee et al., 2012; Azdarpour etl., 2014; Yu et al., 2019), typically as a means to repurpose the gypsum that is produced as industrial waste. However, there is little published work exploring the potential of subsurface gypsum rock for geologic carbon sequestration. By use of Crunchflow reactive transport modeling, this study seeks evaluate the potential of $CO_2$ storage in gypsum-rich subsurface reservoirs. These models will predict the potential mineral dissolution and precipitation reactions as well as the changes in

porosity and ion concentrations that could occur if $CO_2$ were injected into the sample for the first 10,000 days of the injection period.

Specifically, this study seeks to answer the following research questions:

- *What mineral dissolution and precipitation reactions will occur over a 27-year injection period for a formation rich with gypsum minerals?*
- *How will porosity, ion concentrations, pH, and mineral volume fractions evolve over a 27-year injection period?*
- *Will $CO_2$ mineral trapping occur during the injection period?*

### 1.6 Experimentally determining the nature of gypsum in conditions relevant to geologic carbon sequestration.

Batch experiments coupled with simulations in Yu et al (2019) considered the evolution of gypsum subject to conditions relevant to carbon storage. Focused on the coupling of gypsum dissolution to $CaCO_3$ precipitation as a function of brine fluid composition, observations from these experiments suggest that gypsum solubility is independent of both pH and $CO_2$ partial pressure (Yu et al., 2019). However, these experiments were carried out in basic conditions with a maximum partial pressure of 30 bar $CO_2$. There is a lack of research published analyzing the stability of gypsum in high pressure, low pH systems such as deep saline aquifers like the potential injection site located in Cassville, Georgia. Recalling equations 1-4, as $CO_2$ is added to a reservoir in the presence of brine, conditions become highly acidic (pH ~3-3.3). The pressure of the formation at this depth is over 100 bar. To confirm that gypsum remains stable in these conditions, a set of experiments were developed at the temperature, pressure, and $pCO_2$ conditions specific to this potential injection site.

Here, Parr batch reactor experiments were used to validate the stability of gypsum in the presence of $CO_2$ at high pressure, high temperature, and low pH. Simply put, it seeks to answer the question of whether gypsum will dissolve, precipitate, or remain stable when subject to these conditions. The first experiment conducted was using pure gypsum, the second using the same gypsum-rich sample from Cassville, GA analyzed in Chapter 2 (Sample 9). The concentration of calcium ions in solution was collected and analyzed from the experimental system and used to calculate the amount of dissolved gypsum. Scanning electron microscopy images were taken before and after experiments to observe qualitative differences between the reacted and unreacted samples.

This study seeks to answer the following research question:

- *Will gypsum dissolve in the presence of $CO_2$ saturated brine at conditions relevant to geologic carbon sequestration?*
- *What qualitative differences can be observed between the reacted and unreacted samples?*

# Chapter 2. Reactive transport modeling of subsurface gypsum-rich rock in the context of geologic carbon sequestration

## 2.1 Introduction

### 2.1.1 Geologic Carbon Sequestration and Gypsum

There is general consensus within the scientific community and society as a whole that the effects of increased $CO_2$ emissions from anthropogenic sources must be simultaneously prevented and mitigated. Since the Industrial Revolution, the concentration of $CO_2$ in the atmosphere has increased by more than 40%. (NAS, 2020). Much of this increase is due to anthropogenic activities, namely the burning of fossil fuels (Vose et al., 2017). In 2019, the burning of fossil fuels accounted for 74% of the United States' greenhouse gas emissions (EESI, 2020). The extraction of fossil fuels to burn for energy has disrupted the natural carbon cycle due to the increase in atmospheric $CO_2$. Currently the extraction and use of fossil fuels is not predicted to decrease since it supplies 80% of the world's energy (EESI, 2020).

Geologic carbon sequestration is a promising means of reducing atmospheric carbon dioxide emissions by capturing $CO_2$ gas and storing it long term in subsurface porous rock. The goal of geologic carbon sequestration (GCS) is to sequester $CO_2$ in an aqueous, solid, or gaseous phase so that it cannot reenter the atmosphere. In this study, a gypsum-rich sample from Cassville, GA is analyzed as a potential injection well for GCS. Deep saline aquifers, such as the location of this potential site, are considered favorable for GCS for several reasons: they have large potential storage space in porous media and saline water is not useful for other agricultural or industrial purposes (Dai et al, 2020).

Many studies have analyzed trapping $CO_2$ emissions via mineral carbonation as a means to repurpose industrial waste byproduct gypsum through mineral carbonation (Lee et al 2012, cite

more) however there is a lack of published works evaluating a gypsum rich evaporite deposit in acidic conditions for GCS. Trapping $CO_2$ in a solid mineral form such as calcite ($CaCO_3$) is an ideal outcome of GCS as it may not re-enter the atmosphere after it has been mineralized. If gypsum ($CaSO_4 \bullet 2H_2O$) dissolves in solution, it could provide an excess in calcium ions to react with the injected $CO_2$ to create calcite. These processes are depicted in equations 6, 7, and 8.

$$CaSO_4 \cdot 2H_2O \leftrightarrow Ca^{2+} + SO_4^{2-} + 2H_2O \quad (6)$$

$$Ca^{2+} + HCO_3^{2-} \leftrightarrow CaCO_3(s) + H^+ \quad (7)$$

$$CaSO_4 \cdot 2H_2O + HCO_3^{2-} \leftrightarrow CaCO_3(s) + SO_4^{2-} + 2H_2O \quad (8)$$

Research suggests that while calcite solubility is highly dependent on pH, gypsum solubility is independent of both pH and $CO_2$ partial pressure.

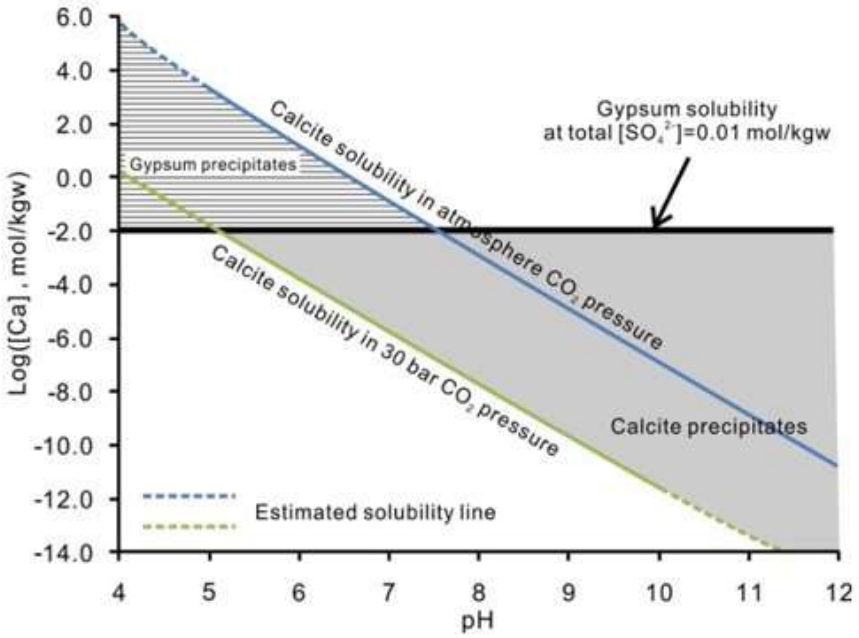


*Figure 4. Calculated values of the logarithm of calcite solubility and logarithm of gypsum solubility in aqueous solutions having a total [SO4 2−]=0.01 mol/kgw and a total NaCl concentration of 0.01 mol/kgw versus fluid pH under atmosphere and 30 bar CO2 partial pressure (Yu et al., 2019)*

This phenomenon was calculated theoretically at 30 bar $CO_2$ partial pressure in a study by Yu et al. (2019) and is depicted in Figure 4. This suggests that the degree to which gypsum converts to calcite is strongly pH dependent; specifically, that is occurs at basic conditions. But as pressure increases, calcite precipitation can occur at more acidic conditions. For example, in Figure 4, at atmospheric pressure, calcite is predicted to precipitate at pH > 7.5, but at 30 bar, calcite is predicted to precipitate at pH > 5.1. Therefore, as pressure increases, calcite precipitation could occur in more acidic conditions.

In this study, the potential impact of injected $CO_2$ on mineral dissolution and precipitation reactions, porosity of the formation, and ion concentration evolution is investigated in modeling approaches. An initial Crunchflow reactive transport model was developed to predict the initial composition of the aquifer brine. An additional Crunchflow reactive transport model was developed using the simulated brine chemistry results to simulate the flow and transport of $CO_2$ through this aquifer in a micro-continuum scale.

## 2.2 Methods

### 2.2.1 Sample Background

The sample analyzed in this study (Sample 9) was taken from a Cassville stratigraphic test well located in Cassville, Georgia. An optical microscope image of the sample is shown in Figure 5 below. The sample is predominantly gypsum with some quartz and dolomite as well as trace amounts of illitie. Table 1 displays the x-ray diffraction (XRD) content of the sample as well as the depth at which the sample was taken.

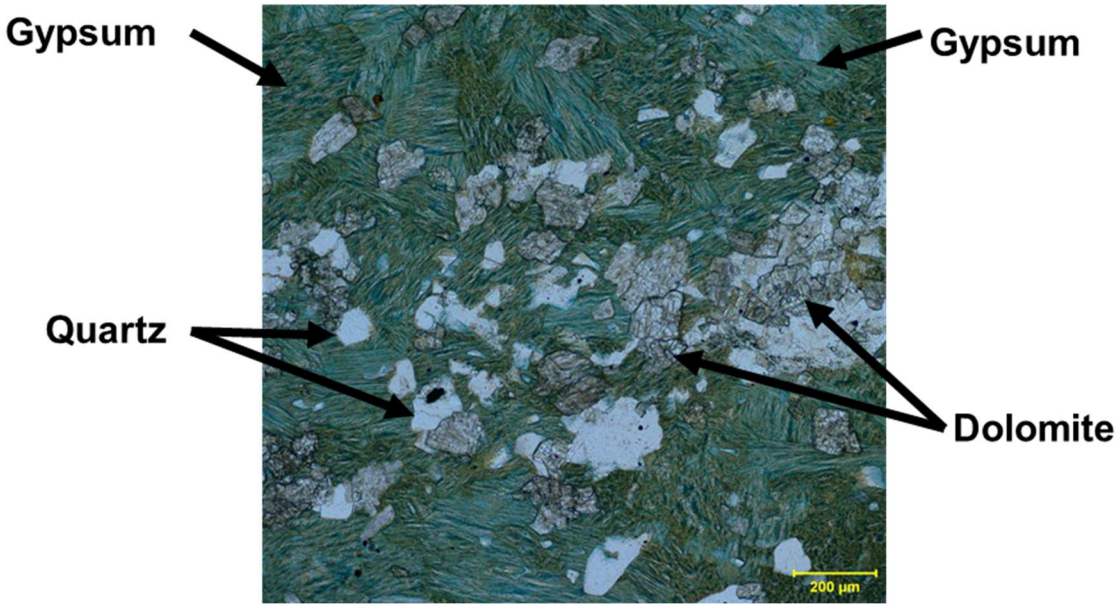


*Figure 5. Optical microscope image of sample analyzed in this study (Schlumberger Reservoir Laboratories).*

| Table 1. Sample Characteristics and Mineral Weight% (Schlumberger Reservoir Laboratories) | | | | | | |
|---|---|---|---|---|---|---|
| Depth (ft) | Lithotype | Quartz | Dolomite | Illite*Mica | Gypsum | Anhyrdrite |
| 3866.97 | gypsum | 7.0% | 12.0% | 1.0% | 79.0% | 1.0% |

**2.2.2 Scanning Electron Microscopy**

Scanning electron microscopy (SEM) images were collected of polished thin sections and utilized to obtain the porosity of the sample for subsequent reactive transport simulations. 2D SEM back-scatter electron (BSE) images were taken in this study on polished sample thin sections using a Zeiss EVO10 Scanning Electron Microscope in variable pressure mode. As the sample is non-conductive, the sample was first gold coating using a Sputter EMS150R Plus Rotary Pumped Coater. BSE images are particularly useful to segment pore and mineral phases as phases appear brighter with increasing atomic weight such that mineral phases are lighter in grayscale and pore spaces appear black.

The image was segmented into a binary image in ImageJ using a threshold value of 68 to differentiate the pores from the gypsum grains. This threshold value was determined through a qualitative visual analysis of pores versus grains, differentiated by black and grayscale pixels respectively. After that, ImageJ data processing was used to calculate the percentage of black space (i.e. pores).

### 2.2.3 Brine Chemistry Model Development

Before creating a Crunchflow model to predict the injection of $CO_2$ into this sample, a brine chemistry model was developed in Crunchflow to predict the initial state of the aquifer. Specifically, this was a batch equilibrium model to predict the initial composition of the brine, pH of the system, and ion concentration levels based on equilibrium of the fluid with the formation mineralogy at the formation temperature and pressure conditions. To ensure equilibrium was achieved, this model was run for 10,000 years. The saline brine was modeled as 1 molar NaCl. The temperature of the aquifer was estimated at 35.0ºC based on a temperature gradient of 15ºC/km from United States Geological Services data for the state of Georgia and the average surface temperature of 17.34ºC from the national weather service (USGS, 1987). The formation pressure was estimated to be 123 bar based on a pressure gradient of 105 bar/kilometer (Crandell et al., 2009). To account for ion strength, Crunchflow employs the Debye–Hückel formulation to calculate the activity coefficients for each ion. This model predicted the initial concentration of each ion in the brine from the following data from each mineral: volume percent normalized by the porosity of the sample, specific surface area, and dissolution rate constant for acidic conditions. This input data is displayed below in Table 2.

| Table 2. Brine Chemistry Model Input Data | | | |
|---|---|---|---|
| **Mineral** | **Volume %** | **Rate Constant** | **Average SSA ($m^2/g$)** |
| Gypsum | 61.18 | -14.54 | 0.5764 |
| Dolomite | 7.46 | -5.597 | 0.1547 |
| Quartz | 4.70 | -11.83 | 0.1064 |
| Illite | 0.64 | -14.34 | 93.23 |

The acidic rate constants were interpolated from literature experimental dissolution rate data, under $CO_2$ induced acidic conditions when feasible, to the temperature of the system for dolomite (Gauteiler 1998), quartz (Brady and Walther 1990), and illite (Koheler et al., 2002). Amongst the literature, no dissolution rate constant was found for gypsum as it does not typically dissolve in acidic conditions. The original solution to this problem was to use the default rate constant for gypsum in the Crunchflow database, however this created simulation results that suggest complete dissolution of gypsum. This was considered implausible due to the published research suggesting that gypsum remains stable regardless of pH and partial pressure of $CO_2$ (Yu et al., 2019). As such, an alternative rate constant for gypsum was averaged from a field study of a confined gypsum-rich aquifer approximately 500 meters deep in a hydraulically connected to sandy carbonate beds located in Western Ukraine (Klimchouk at al., 1996; Klimchouk and Askem, 2005). Preliminary simulations showed that use of this rate constant resulted in gypsum remaining relatively stable, agreeing more reasonably with Yu et al. (2019) and as such was selected for the duration of simulations. The specific surface area values for each mineral phase were also collected from literature. High and low Brunauer-Emmett-Teller (BET) adsorption obtained specific surface area values were averaged for gypsum (Tang et al., 2018), dolomite (Porkrovsky et al., 2005), quartz (Brady and Walther, 1990), and illite (Koehler et al., 2002).

### 2.2.4 Flow and Transport Model Development

The second Crunchflow model developed was a one-dimensional flow and transport model to simulate the injected $CO_2$ traveling through the aquifer. The goal of this model was to predict the geochemical processes that could occur if this site was chosen for GCS injection, namely the changes in mineral volume fraction, porosity, and ion concentration over a 27-year injection period across a 38-meter path. This time length was chosen as a typical injection period for a project of this scale (Vilarassa et al., 2014; Congressional Research Service, 2022). The length of the model was chosen based on the flow rate, 0.38 meters per day. This flow rate was found from a field study that collected flow rate data through dolostone aquifers (Voors et al., 2009). This was most appropriate considering the well is predominately dolostones, with this particular sample being the one anomaly.

Additionally, this model sought to evaluate the potential for $CO_2$ mineral trapping. As $CO_2$ gas is injected into the well, it reacts with brine as well as the aquifer minerals. This simulation models interactions of brine saturated with $CO_2$ traveling through the mineral cells in the saturated zone adjacent to the $CO_2$ plume. This is anticipated to be the most reactive zone in terms of promoting mineral dissolution reactions. The schematic of the model system is depicted in Figure 6.

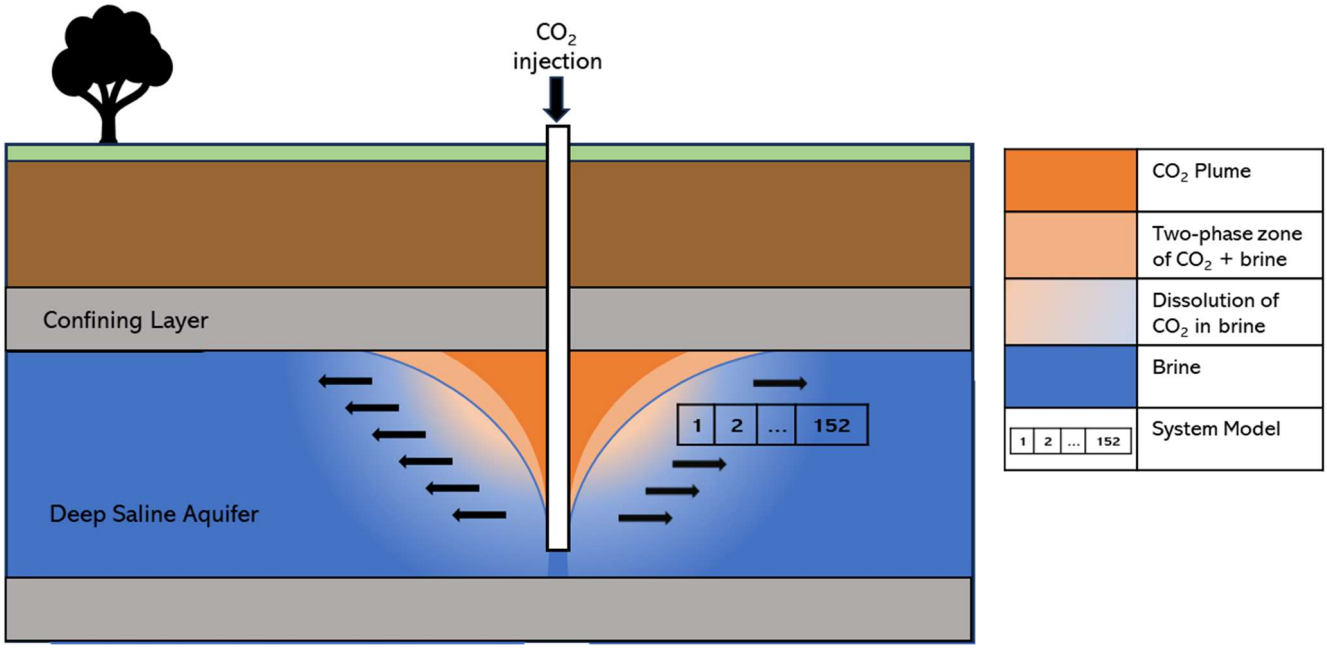


*Figure 6. System schematic depicting the flow of injected $CO_2$ gas through deep saline aquifer in the presence of brine. Also depicted is the conceptualized location of the RTM system grid cells.*

In Crunchflow, discretization of a grid is required to simulate flow and transport. For this one-dimensional model, a single row of grid blocks was defined in the x direction. There is a total of 152 0.25-meter cells, the first being a "ghost cell," meaning it was comprised solely of the original brine predicted by the brine chemistry model in equilibrium with $CO_2$. This allows the simulated injected $CO_2$ to react with the original brine preceding its interaction with the mineral grid cells. A schematic of this model is shown below in Figure 7.

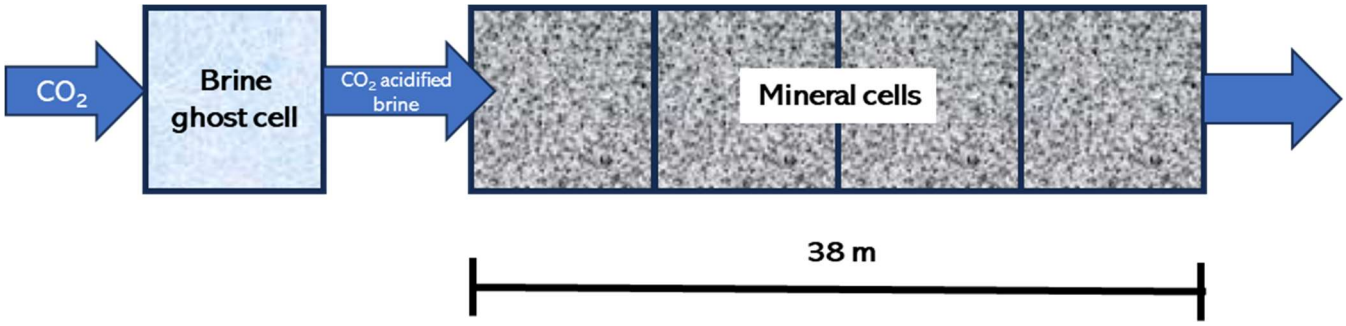


*Figure 7. Schematic of flow and transport model.*

Separate initial conditions were defined for the ghost brine cell and the mineral cells. For each condition, the temperature, pH, ion concentration, mineral volume percentage and mineral specific surface areas were required. Throughout the model, the temperature was set to the formation temperature of 35.025ºC, the pH determined based on charge balance, and the initial ion concentrations based on the results from the brine chemistry model depicted in Table 3. In the ghost cell, the formation brine was equilibrated with $CO_2$ present at a partial pressure of 100 bar using the Duan and Sun equation of state for $CO_2$ (Duan and Sun 2006). The mineral volume percentages and specific surface areas were all set to zero in this cell. For initialization of the mineral cells, mineral volume percentages and specific surface areas were set to the values listed in Table 2 and the system was assumed saturated with the simulated formation brine (Table 3). Calcite was added to the model as a potential secondary mineral to consider possible calcite precipitation and subsequent dissolution.

A flow rate of 0.38 meters per day was used in this model. This was estimated from literature values for similar carbon injection systems (Voorn et al., 2015). The model simulated a 10,000-day (~27 year) injection period. Longer models were developed; however, this time frame was chosen to best represent the extent and rate of the short-term reactions as they are the most

significant change in the system. During each time step and at each location, the mineral volume fraction, ion concentration, and porosity were tracked.

## 2.3 Results and Discussion

### 2.3.1 Scanning Electron Microscopy

The collected SEM images are given in Figure 8 and 9. Gypsum is extremely fibrous, and its porosity exists on a very fine scale (Fig. 8). Examination of the SEM images shows that gypsum is the most abundant mineral and occupies space between the dolomite and quartz grains such that there is no observable additional pore space. As such, it is assumed that the porosity of the sample is entirely from the gypsum. Therefore, another BSE image was taken from a region of the sample that was entirely gypsum to better discern the porosity (Figure 9). After undergoing image segmentation and data analysis in ImageJ (Fig. 10), the resulting porosity is 26%, which is in the middle of gypsum porosity values collected from the literature of 21% (KGS, 2017) and 32% (Kong et al., 2018).

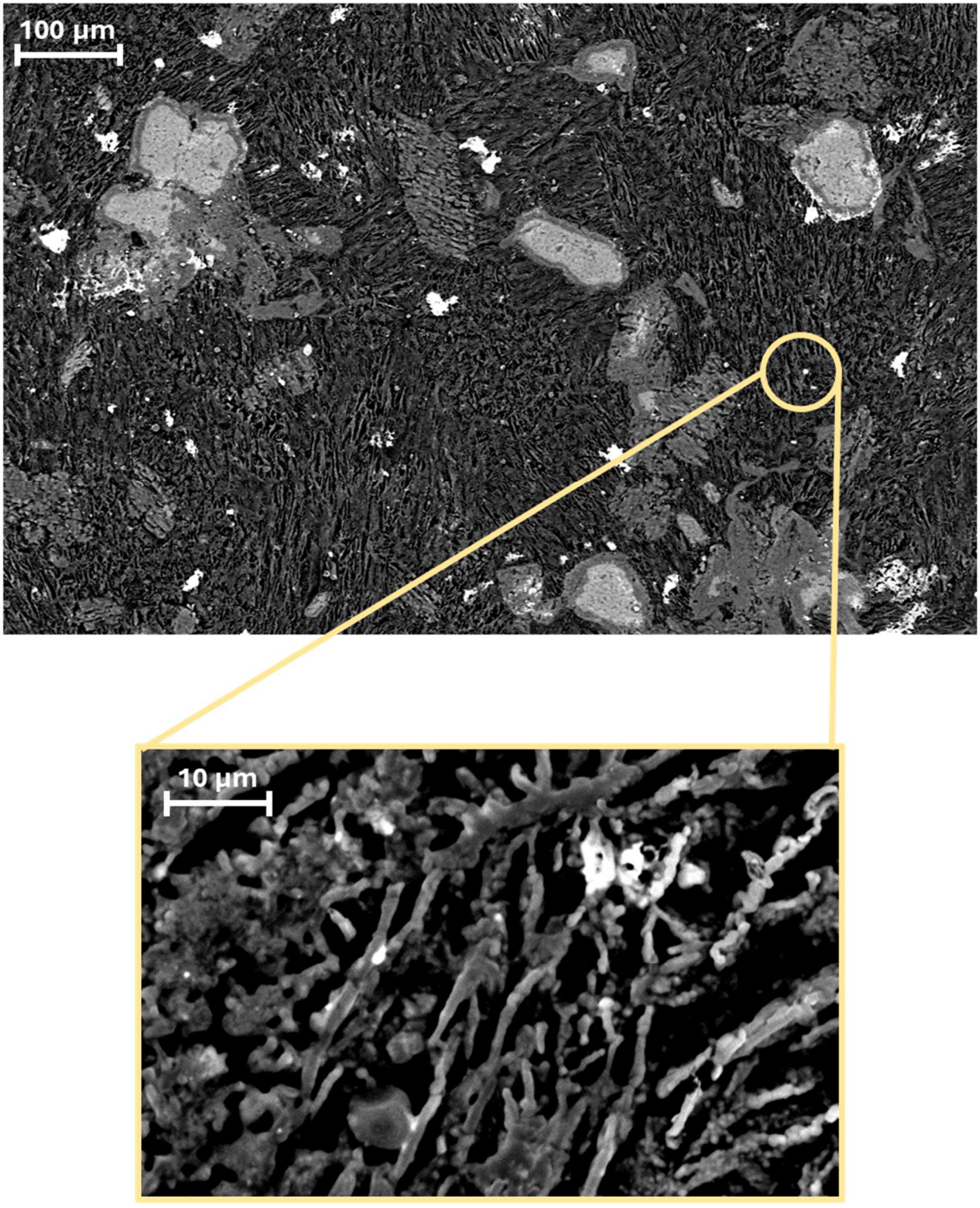


*Figure 8. Two BSE SEM images of sample 9 at different resolutions.*

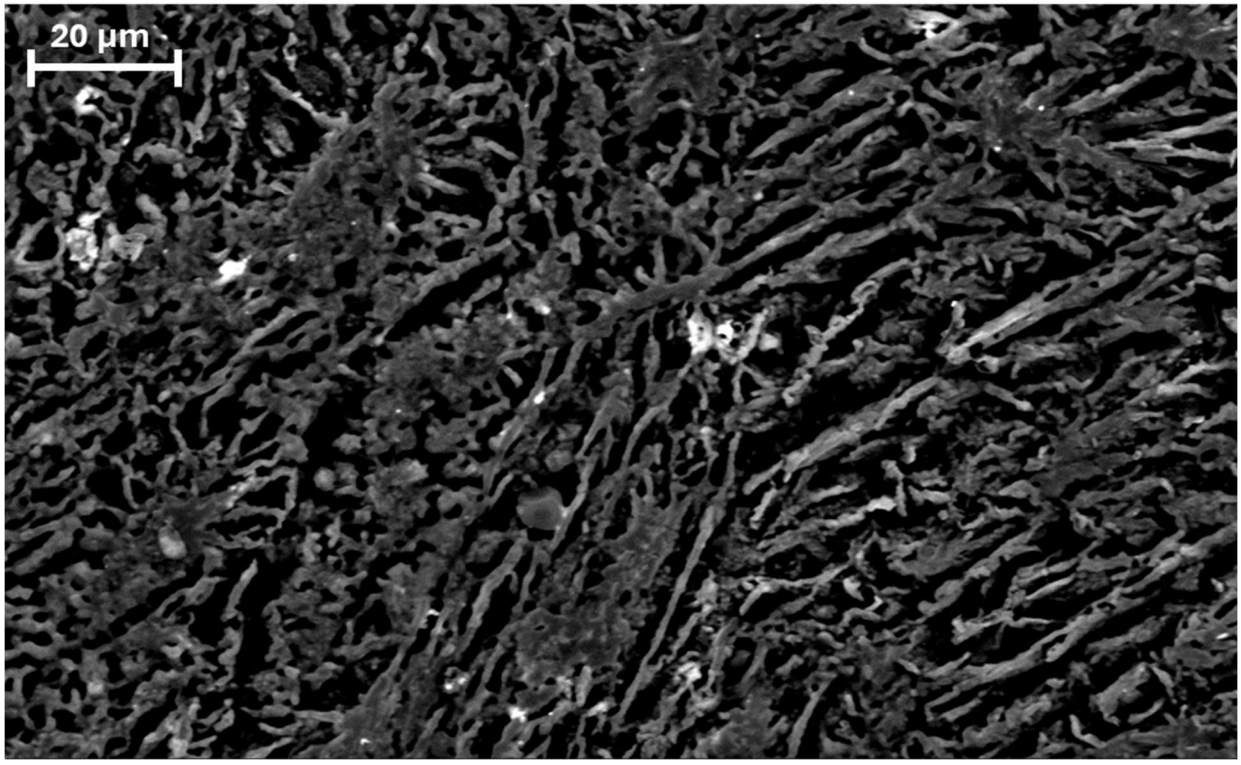


*Figure 9. BSE Image of gypsum region used for porosity analysis.*

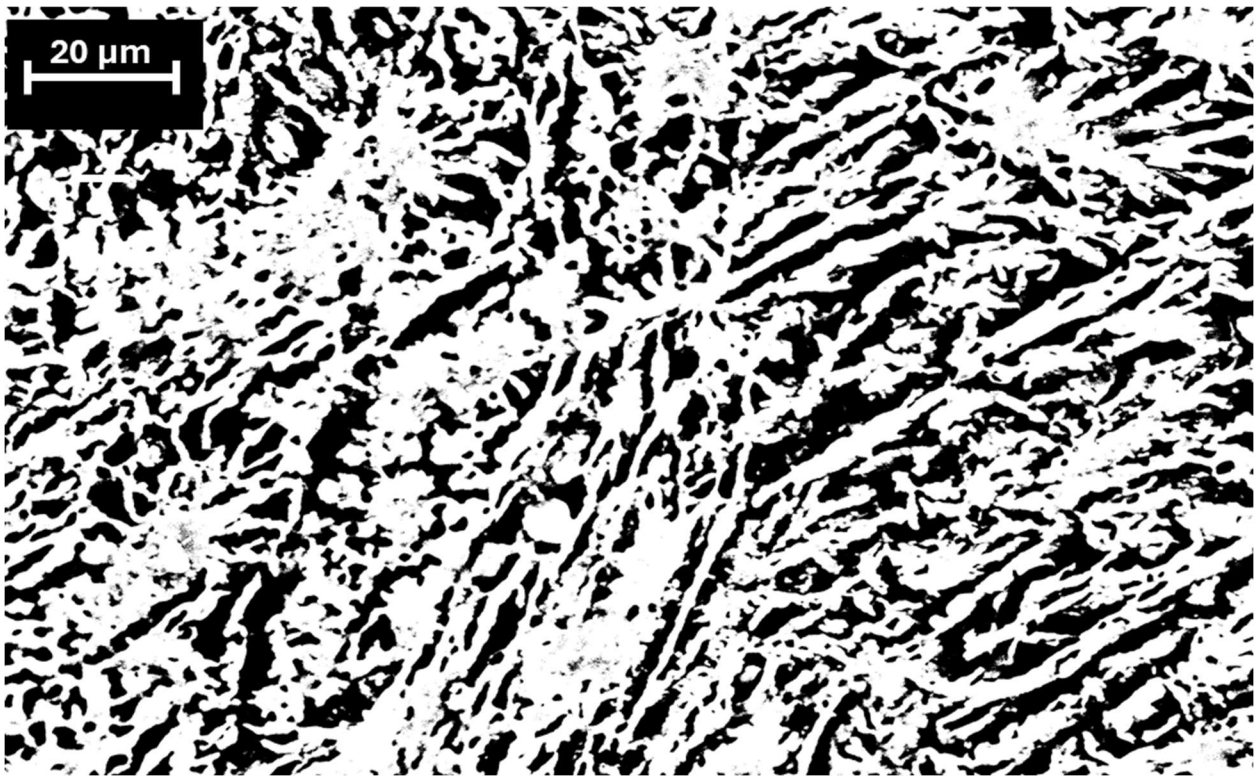


*Figure 10. Segmented gypsum region used for porosity analysis.*

### 2.3.2 Brine Chemistry Model Results

The results from the brine equilibrium model are displayed in Table 3. These data serve as inputs for the secondary flow and transport model. Calcium and sulfate are the ions in highest abundance, which is reasonable considering the sample is predominantly gypsum. There is smaller amounts of aqueous silica and magnesium, from the quartz and dolomite minerals in the sample, respectively, and trace amounts of aluminum and potassium from the illite. The simulated pH of the formation brine is 8.55.

**Table 3. Brine Chemistry Model Results**

| **pH** | **[$Na^+$]** (mol/kg) | **[$Cl^-$]** (mol/kg) | **[$SiO_2(aq)$]** (mol/kg) | **[$Al^{3+}$]** (mol/kg) | **[$Ca^{2+}$]** (mol/kg) | **[$SO_4^{2-}$]** (mol/kg) | **[$Mg^{2+}$]** (mol/kg) | **[$K^+$]** (mol/kg) |
|---|---|---|---|---|---|---|---|---|
| 8.55 | 1 | 1 | $2.82 \times 10^{-4}$ | $2.06 \times 10^{-6}$ | $3.36 \times 10^{-2}$ | $3.35 \times 10^{-2}$ | $9.65 \times 10^{-5}$ | $5.36 \times 10^{-7}$ |

### 2.3.3 Flow and Transport Model Results

For the first 50 days of injection, the simulated evolution of formation minerals in the first mineral grid cell is shown in Fig. 11, porosity in Fig. 13, and evolution of ions in solution in Fig. 15. Figures 12, 14, and 16, respectively, display these data over the full 27-year time scale. In all these figures, flow of $CO_2$ acidified brine begins at a time of zero days and the negative time reflects the initial condition of the system before injection of $CO_2$.

The results from the simulation indicate that under the simulation conditions, gypsum remains relatively stable (Fig.11, 12). There is slight gypsum dissolution over the entire 27-year period, evident from the decrease in gypsum volume percentage in Fig. 11 (from 61.18% to 61.17%). This dissolution slightly increases the calcium concentration, shown in Figure 15. Slight quartz precipitation occurs over the 27-year period as indicated by the increase in volume percentage in Figure 11 (from 4.70% to 5.33%) which decreases the aqueous silica in solution in

Figure 15. This precipitation is triggered by the slight dissolution of illite indicated by the decrease in volume percentage in Figure 12 (from 0.64% to 0.55%). Illite dissolution throughout the 27-year period increases the concentration of potassium ions in solution in Figure 16. This simulation also suggests rapid and complete dissolution of dolomite within the first 40 days of injection, shown by the sharp decrease of dolomite volume percentage in Fig. 11 and 12 as well as the increase in magnesium and calcium ions in Fig. 15 and 16. The other minerals remain relatively stable within the first 50 days of injection as shown in Fig. 15.

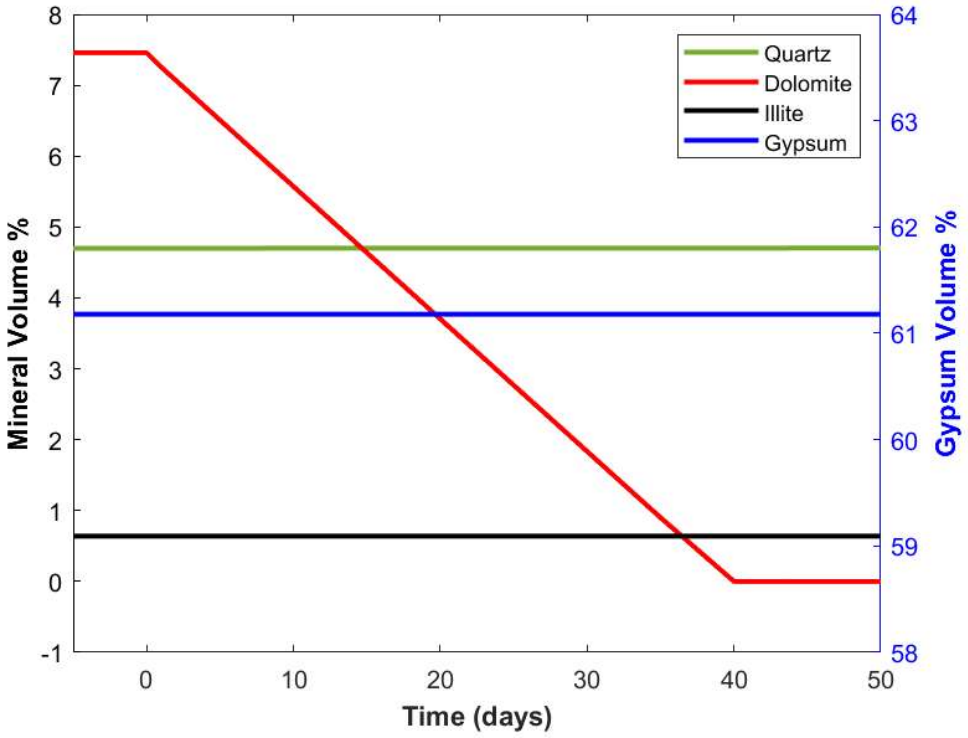


*Figure 11. Simulated mineral volume percentage evolution over the first 50 days of injection.*

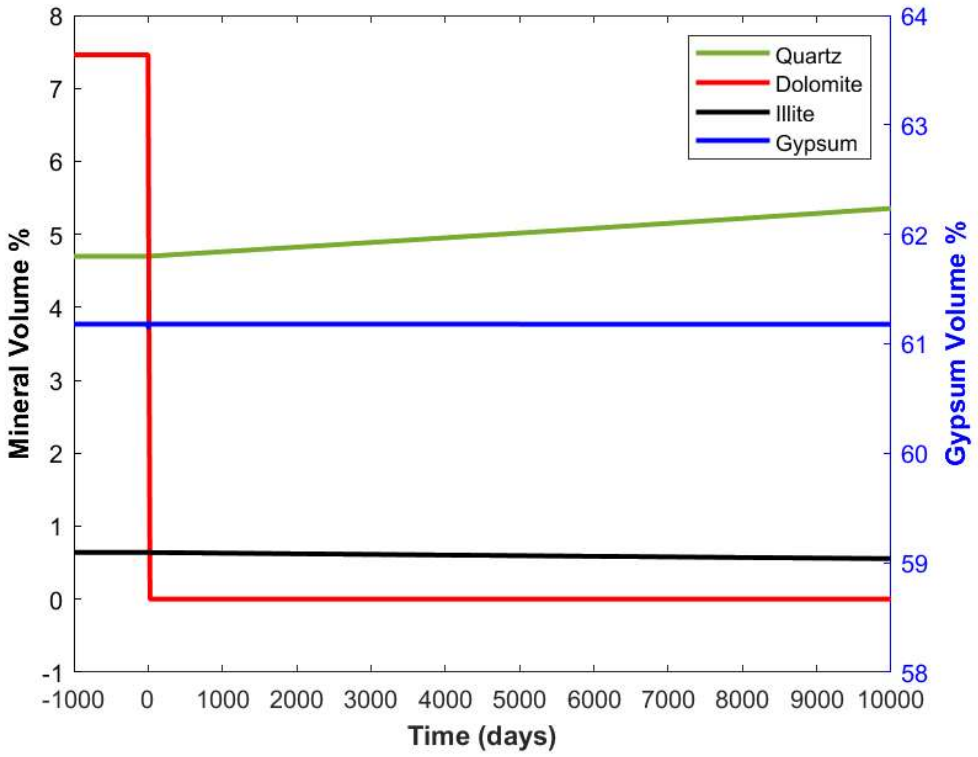


*Figure 12. Simulated mineral volume percentage evolution over the entire 27-year injection period.*

Complete dolomite dissolution occurs within the first 45 days of injection and is the driving force of porosity increase from 26% to 33% (Fig. 14, Fig. 16). Porosity reaches its peak (33.5%) when dolomite is completely dissolved. However, due to slight quartz precipitation, by the end of the 10,000-day period the porosity decreases to 33% (Fig. 13).

The simulated evolution of ion concentrations over the 10,000-day period shows that with the addition of $CO_2$ to the system, the pH plummets to 3.3. There is a sharp increase in magnesium ion concentration as dolomite dissolves before it returns to the background concentration value after dolomite is completely consumed. The amount of silica in solution decreases slightly as there is small amounts of quartz precipitation triggered by illite dissolution over the 27-year injection period. Illite dissolution is evident from the increase of potassium ions in solution.

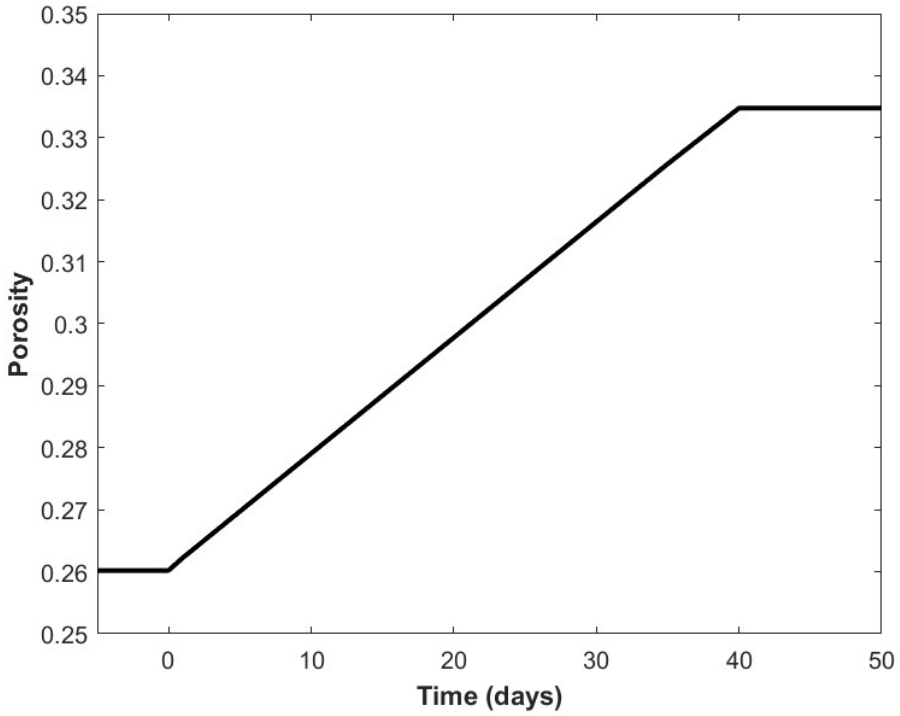


*Figure 13. Simulated porosity evolution over the first 50 days of injection.*

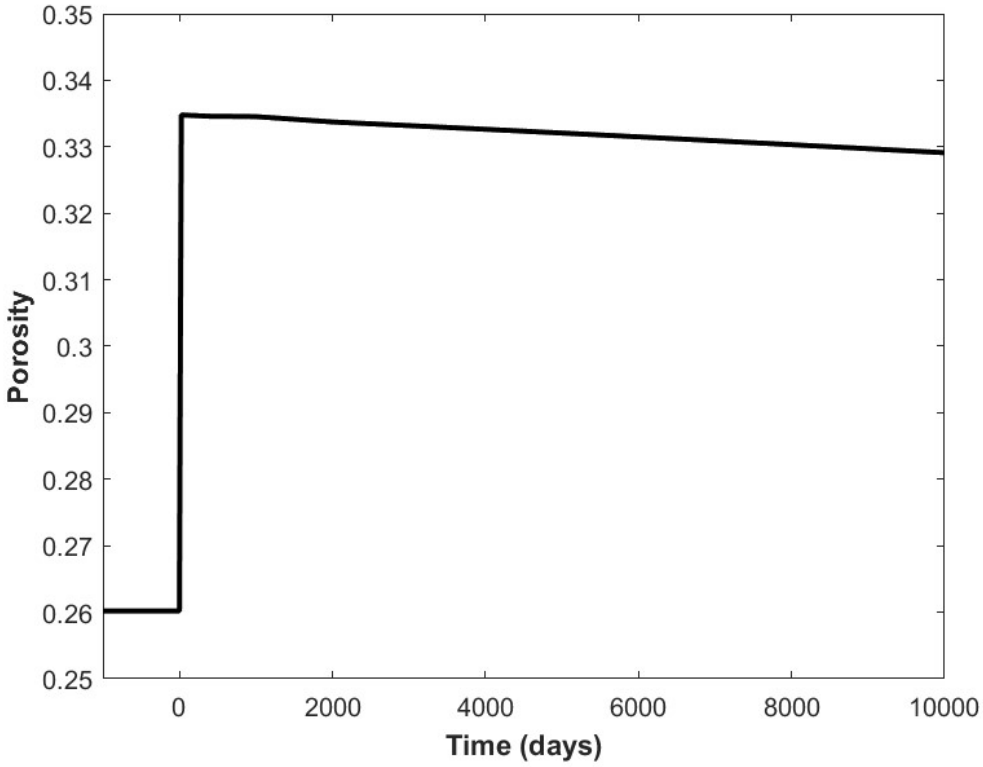


*Figure 14. Simulated porosity evolution over the entire 27-year injection period.*

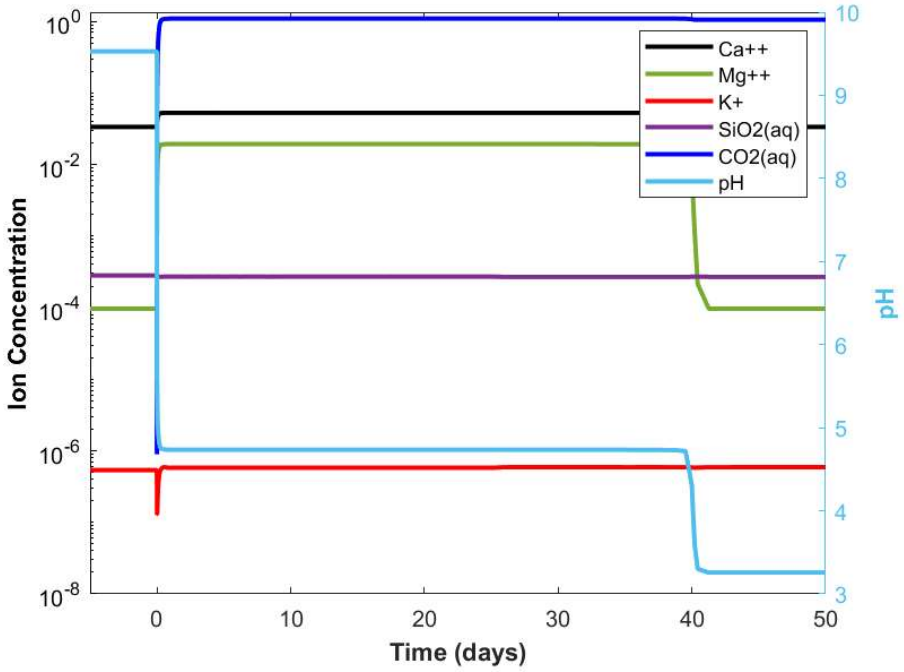


*Figure 15. Simulated ion concentration and pH evolution over the first 50 days of injection.*

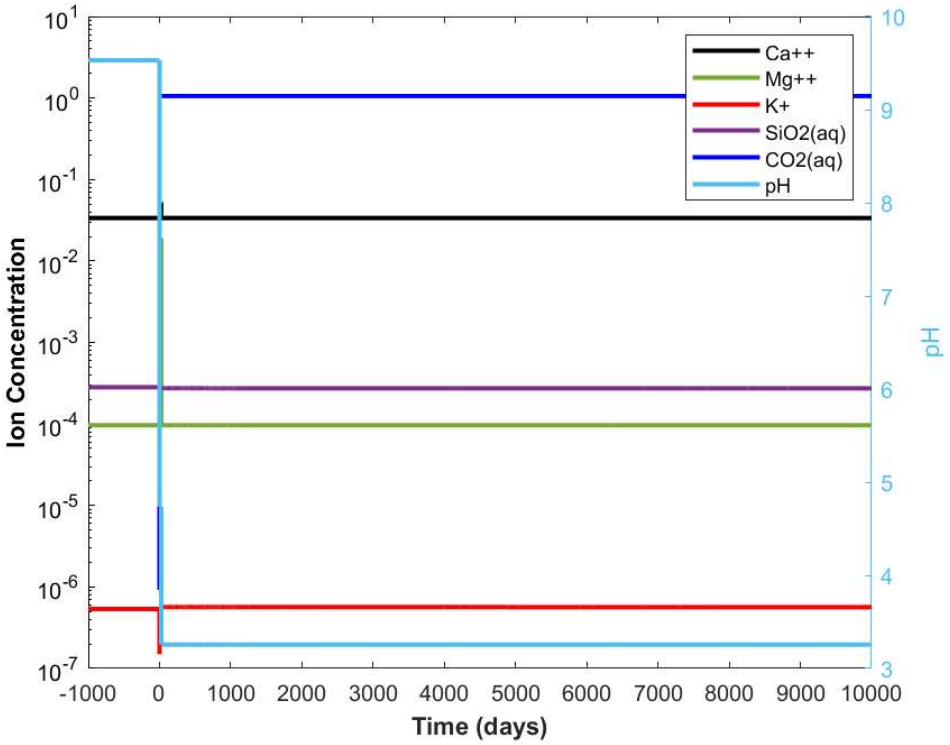


*Figure 16. Simulated ion concentration and pH evolution over the entire 27-year period.*

With the initial increase of calcium ions in solution from dolomite and gypsum dissolution, there is potential for calcite precipitation in this system. However, these simulated results suggest that calcite precipitation will not occur in this formation during the injection period (Fig. 17). Figure 17 shows that the saturation index (SI) of calcite decreases to -3.5 within the first 50 days of injection and remains at that level throughout the duration of the 27-year period. This negative SI indicates that if calcite were present in the system, it would be dissolving. Although research suggested that gypsum dissolution can trigger calcite precipitation in more acidic conditions than typical in high pressure environments (Yu et al. 2019), this was not observed in the simulation.

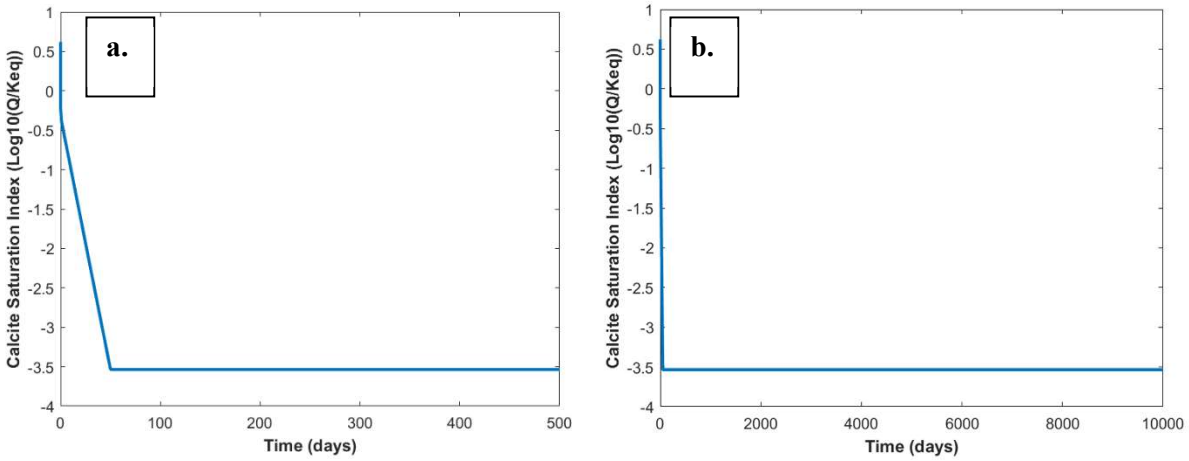


*Figure 17. Simulated saturation index for calcite over (a) the first 500 days of injection and (b) the entire 27-year period.*

Figures 11-17 represent the changes occuring in the first grid cell, those directly adjacent to the simulated equilibrium brine-$CO_2$ boundary. Figures 18-20 display the changes in porosity, dolomite volume percentage, and pH over time at increasing distances away from the plume, throughout the entire simulated length (0.125 meters, 3.88 meters, 13.5 meters, 23.4 meters, and 38 meters). Dolomite evolution was chosen to represent the transport of geochemical processes

occuring generally in the system since it is the driving factor of porosity increase in the sample, buffers the pH of the system, and undergoes the most drastic transformtion.

Like the phenomenon displayed in Fig. 11-14, Fig. 18 and 19 suggest that the porosity increase of the sample is a direct result of the dolomite dissolution regardless of the distance away from the injection site. The porosity increase occurs simultaneously with the dolomite dissolution at each distance. These figures also suggest the upstream dolomite must be consumed before downstream dolomite dissolution occurs.

Dolomite dissolution throughout the system buffers the pH (Fig. 20). Initially, with the injection of $CO_2$ the pH of the system drops to 4.7. The pH at a distance remains buffered at this level until dolomite dissolution occurs at that said distance, at which point it decreases further to 3.26.

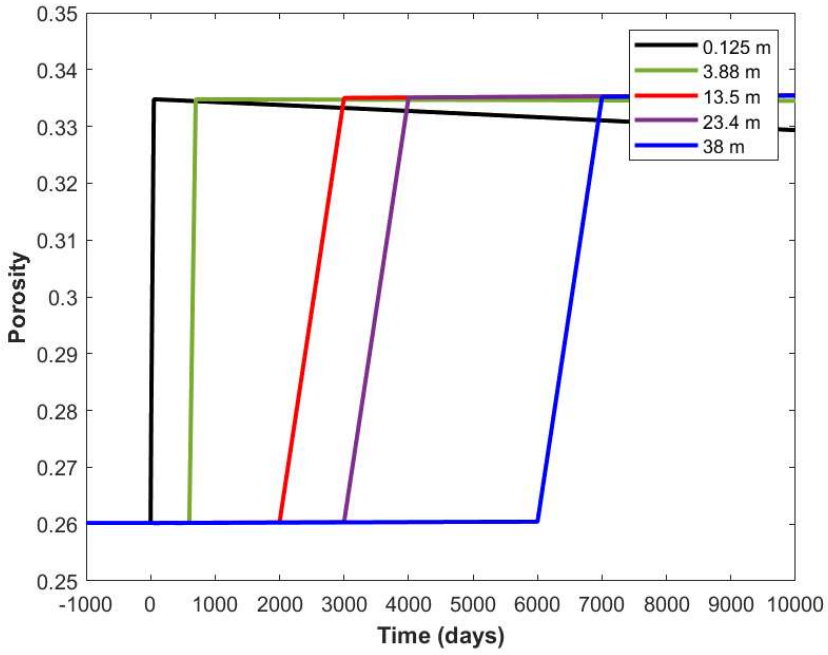


*Figure 18. Simulated porosity evolution at various distances.*

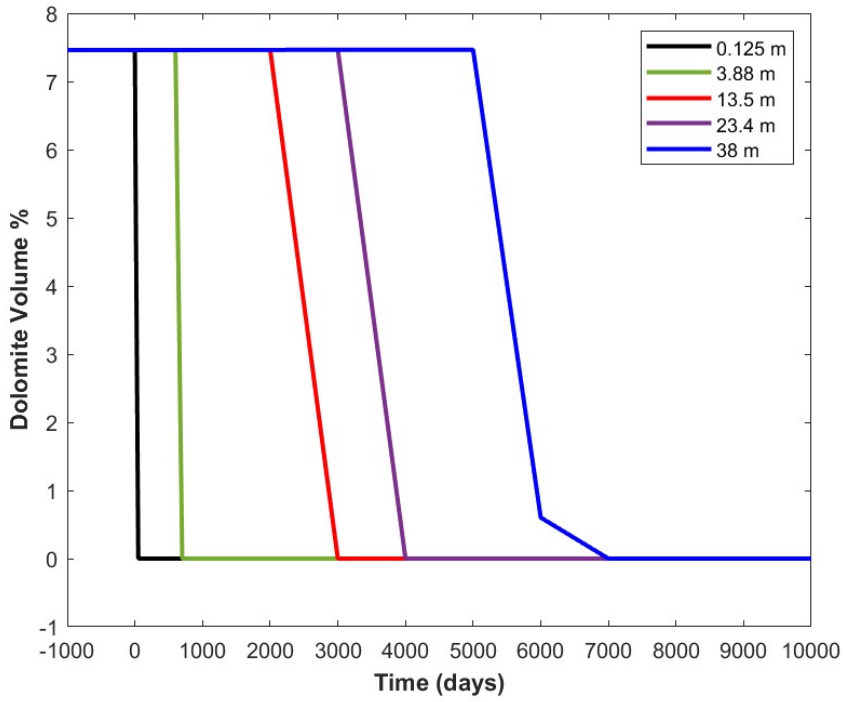


*Figure 19. Simulated dolomite volume percentage evolution at various distances.*

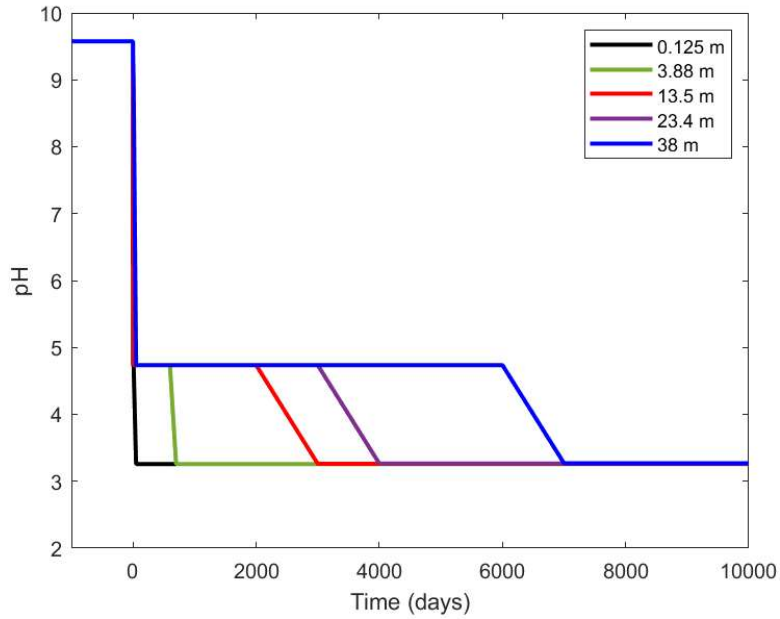


*Figure 20. Simulated pH Evolution at various distances.*

## 2.4 Conclusion

In this work, injection of $CO_2$ into a gypsum-rich sample from a formation in Cassville, GA was considered. 2D SEM images of this sample reveal the fibrous nature of this sample with

ample porosity for potential $CO_2$ storage. Micro-continuum scale reactive transport simulations were then developed and used to simulate the impact of geochemical reactions following injection of $CO_2$ on the fate and transport of injected $CO_2$. The simulations suggest that injection of $CO_2$ would result in a limited extent of mineral reactions. Simulations show rapid dissolution of dolomite which increases the porosity of the formation. However, as this mineral is only present at 7.46v%, the porosity increase is limited. In addition, dissolution of illite results in subsequent quartz precipitation which further limits increases in porosity. In terms of gypsum, limited reaction is expected, and simulations suggest gypsum will remain stable throughout the duration of $CO_2$ injection. To confirm the validity of the mineral volume evolution displayed in these models, namely the stability of gypsum, a series of experiments are developed and conducted in Chapter 3.

The rate and extent of reaction, and subsequent porosity alteration, vary with the distance away from the $CO_2$-brine plume interface. The largest extent of reaction occurs in the mineral cell closest to the plume. Dissolution reactions in this cell increase ion concentrations in solution, limiting subsequent downstream dissolution. Once the upstream dolomite is consumed, however, dolomite rapidly dissolves downstream, increasing porosity. This model suggests that for the domain, there is a peak porosity value of 33.5% which then decreases to 32.9% due to slight quartz precipitation.

In terms of the $CO_2$ trapping mechanisms, this simulation suggests limited mineral trapping in the injection period in this sample; however, it cannot speak to the potential of mineral trapping in the post-injection period or surrounding dolostones. No calcite precipitation was observed in this simulation. Although mineral trapping via calcite precipitation is considered a permanent form of carbon sequestration, such reactions may decrease reservoir permeability and limit the amount

of carbon stored. The fact that simulations suggested conditions were not favorable for formation of secondary minerals implies that such permeability reductions will not be anticipated here during the injection period. Instead, permeability is anticipated to increase during the injection period given the observed increase in porosity from dolomite dissolution. This will be favorable for maintaining injectivity but may result in a larger plume footprint.

# Chapter 3. Experimentally determining the nature of gypsum in conditions relevant to geologic carbon sequestration.

## 3.1 Introduction

As indicated in Chapter 2, the validity of the flow and transport model relies on an accurate understanding of how gypsum will react in the context of the high pressure, high temperature, and low pH conditions of a deep aquifer in the presence of $CO_2$. This study seeks to evaluate the stability of gypsum observed via simulation in the previous chapter by means of Parr batch reactor experiments in conditions pertinent for the storage formation. There are studies analyzing gypsum in the context of GCS in basic conditions (Yu et al., 2019), studies analyzing predominantly carbonate reservoirs with trace amounts of gypsum (Garcia-Rios et al., 2014), and studies analyzing $CO_2$ trapping mechanisms via mineral carbonation of industrial waste byproduct gypsum through mineral carbonation (Lee et al 2012, Song et al., 2014). However, there is little published work analyzing a gypsum-rich formation in acidic conditions as pertinent for geologic $CO_2$ sequestration. It is critical to understand the behavior of gypsum in high pressure and temperature systems under acidic conditions since the addition of $CO_2$ to the system will cause the pH to drop to ~3. This study seeks to provide an overview of the physical behavior of gypsum in such deep saline aquifers injected with $CO_2$.

Two sets of experiments and models were developed. The first was to evaluate the nature of pure gypsum in the context of GCS, the second evaluated the gypsum-rich Cassville, GA sample 9 which was the focus of the simulations in Chapter 2. Experiments exposed both samples to $CO_2$ acidified brine at temperature and pressure replicating field conditions and evaluated the concentration of calcium ions in the effluent solution to quantify the amount of gypsum that dissolved during the experiments. SEM imaging was utilized to display morphological differences

between the initial and final samples used in the experiments. Additionally, 2D SEM images were taken of the samples before and after experimentation to observe qualitative differences.

## 3.2 Methods

### 3.2.1 Pure Gypsum Experiment Design

The experiment conducted was for a pure gypsum powder sample (EDTA purity >= 99%). 500 milliliters of 1 M NaCl brine was placed in a Parr 4848 Reactor along with 100 grams of pure gypsum in a fine powder. The reactor was set to system conditions: $CO_2$ was pumped into the reactor until it reached 100 bar partial pressure and the temperature was increased to 35ºC (Fig. 19).

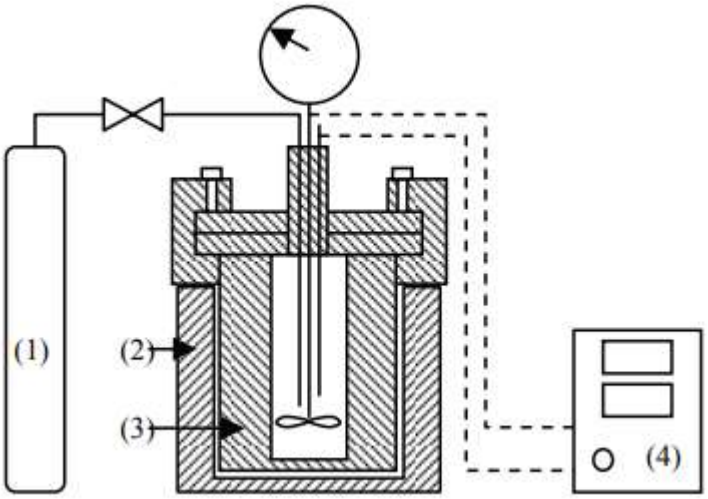


*Figure 21. Experimental design schematic. (1) $CO_2$ cylinder. (2) Heater. (3) 1000-mL high pressure and temperature reactor. (4) Temperature, pressure, and rotation controller. Modified from Onsri et al. (2010).*

The experiment was run for one full week. This time frame was chosen after preliminary Crunchflow simulations suggested the mineral dissolution would take place within the first 200 hours. The conditions of the system are based upon the calculated conditions of the Cassville, GA well used in the RTMs of Chapter 2.

After one week passed, the resulting effluent brine was filtered through a 0.2 μm syringe filter and diluted 10X, 100X, 200X, and 1000X with 0.01 M hydrochloric acid to keep the solution acidic when it returned to atmospheric pressure. The solids from the reactor were rinsed with deionized water and filtered over a flask with gravity as the driving force for one full week. The remaining solids were imaged using the Evo 10 Scanning Electron Microscope.

### 3.2.2 Cassville, GA Sample 9 Experiment Design

A similar approach was used to conduct the Sample 9 batch experiment (Fig 19). However, the experiment was limited greatly by the small amount of sample available. 50 milliliters of 1 M NaCl brine was placed in the Parr 4848 Reactor with 2.34 grams of Sample 9 ground into a powder. The reactor was then heated to formation temperature of 35ºC and then pumped with $CO_2$ until it reached a partial pressure of 100 bar. The reactor was left in this state for one full week to react.

After one week, the sample brine was filtered first through a 0.4 μm syringe filter and then again through a 0.2 μm syringe filter. Due to the small sample size and more dissolution shown, filtration with a wider pore was necessary before fine filtration occurred. As in the first experiment, the brine was then diluted with 0.01 M hydrochloric acid to keep the solution acidic in atmospheric pressure. The solids were also rinsed with deionized water and left to filter into a flask for one full week before being imaged using the SEM.

### 3.2.3 Ion Chromatography

The diluted resulting brine from both experiments was analyzed via ion chromatography (IC). A Thermo Scientific Dionex Aquion ion chromatograph was used with the 6-cation column. IC is a method for separating ions based upon their interactions with resin (stationary phase) and the eluent (mobile phase). The cations move through the column at differing speeds depending on

their affinity for the stationary phase and separate themselves by ion size and charge. As the mobile phase (in this case 0.02 M methanesulfonic acid) travels through the column, the ions with a weaker affinity for the stationary phase will move through faster than the ions with a stronger affinity for the stationary phase. The chromatograph results from the IC plot conductivity versus time with each ion producing a separate peak the height of which correlates to the relative ion concentration at the known time it takes for the ion to travel through the column (Harris, 2010). Although the six-cation column provides data for the lithium, sodium, ammonium, potassium, and magnesium concentrations as well, this study focused on the concentration of calcium. This concentration served as the primary data point collection indicating the amount of gypsum that dissolved in the system.

After initially running several different dilutions of both sets of brine through the IC, the 1000x dilution was chosen to serve as the primary sample specimen used for IC analysis. The high concentration of sodium in solution from the 1 M NaCl brine caused the chromatographs from lesser dilutions to be skewed. Three samples of each brine diluted 1000x with hydrochloric acid were ran through the IC and the concentration of calcium ions in solution was interpolated from the calibration curve from the IC standards. It was assumed that calcium ions in solution came only from gypsum dissolution. In addition to the brine samples, blank DI samples were ran at the beginning and end of the IC sequence as well as in between each separate brine sample. This was to ensure there was no trace amounts of calcium in pure DI water as well as to flush the column between samples.

### 3.3 Results and Discussion

#### 3.3.1 Batch Reactor Experiment Results

Table 4 summarizes the results from the Parr batch reactor experiments. For the pure gypsum sample as well as Sample 9, less than 0.1% of the original gypsum sample dissolves when subjected to the system conditions. This suggests that in the conditions of Cassville, GA stratigraphic test well, gypsum would undergo little dissolution with the addition of $CO_2$.

**Table 4. Parr Batch Reactor Experiment Results and Calculations**

| | Averaged [$Ca^{2+}$] (mg/L) | Mass of Dissolved Gypsum (g) | Original Mass of Gypsum (g) | % Remaining in Solid Phase |
|---|---|---|---|---|
| Pure Gypsum | 0.156 | 0.50 | 1000 | 99.95% |
| Sample 9 | 0.029 | 0.0063 | 2.34 | 99.98% |

There is a potential over-estimation of the amount of gypsum dissolved in Sample 9 since dolomite dissolution was not considered as a contributor to calcium ion concentration. The XRD data suggests that the sample is 7.46% dolomite, however because this sample size was so small (2.34 grams), and then also underwent a 1000X dilution, there were no traces of magnesium in the IC to indicate the amount of dolomite was significant. From the DI samples, no calcium was detected in from the IC above the detection limit of 0.01 mg/L.

### 3.3.2 SEM Imaging

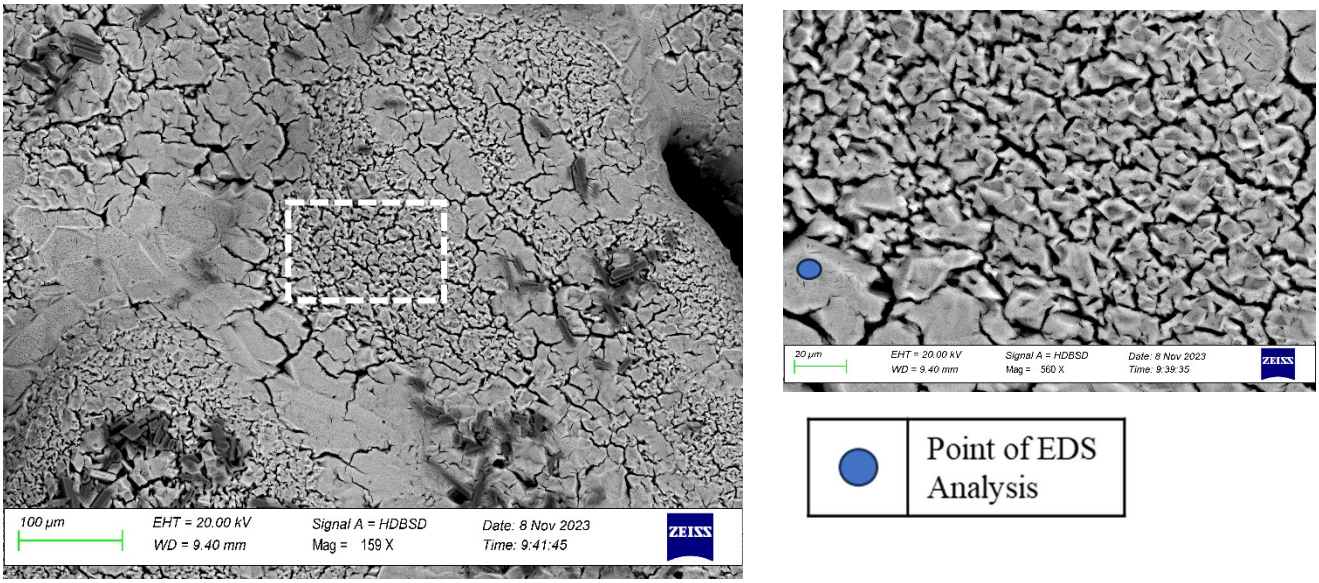


*Figure 22. Unreacted pure gypsum SEM at two separate resolutions. The dotted area displays the area of focus for the right image.*

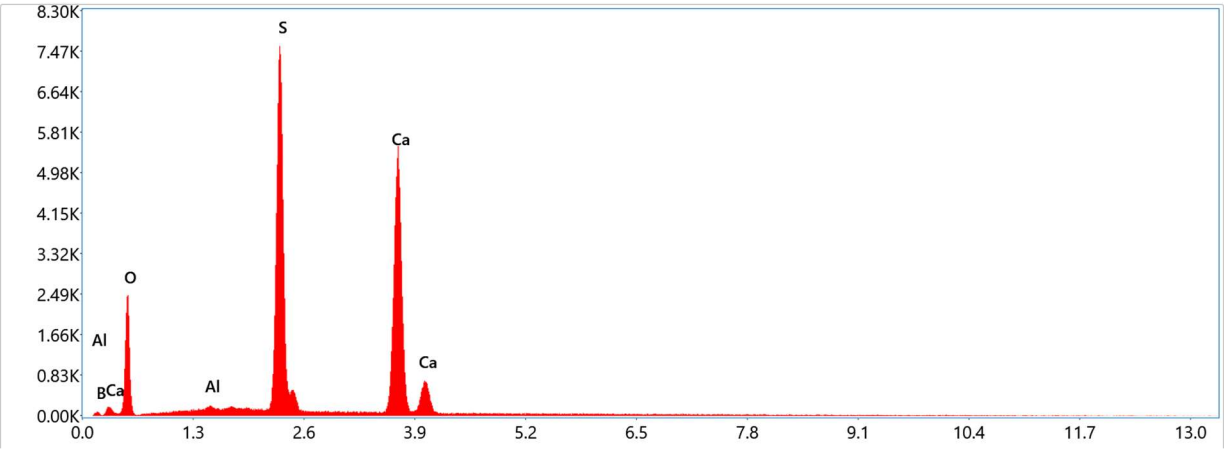


*Figure 23. EDS spot analysis spectra of unreacted pure gypsum sample.*

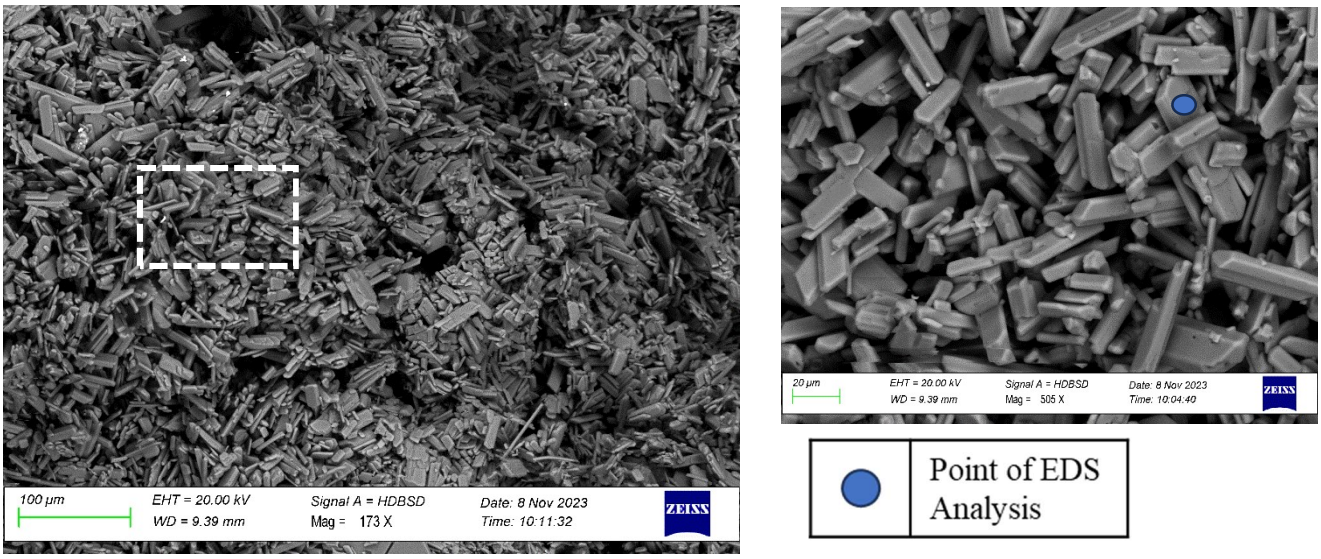


*Figure 24. Reacted pure gypsum sample at two resolutions. The dotted line represents the area of interest for the right image.*

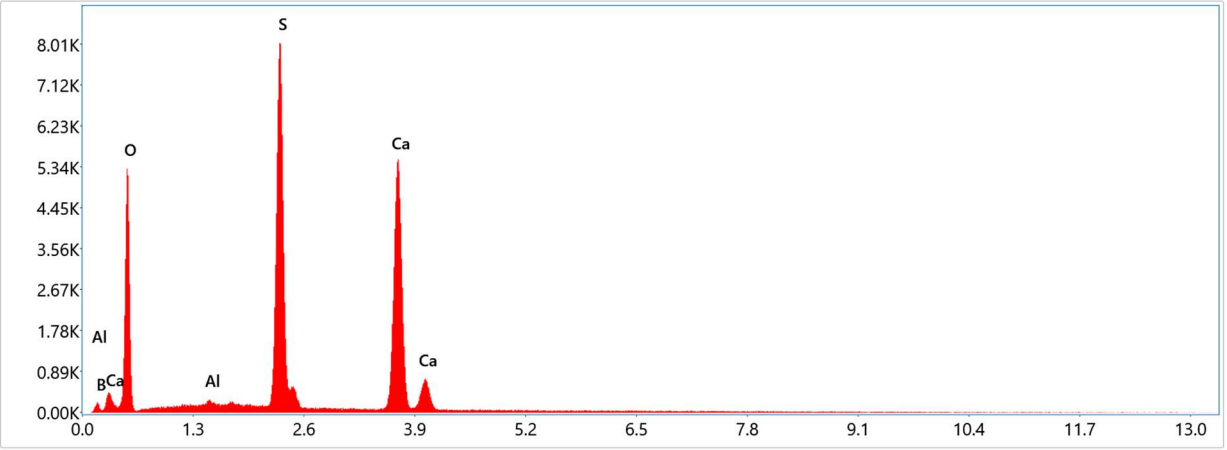


*Figure 25. EDS spot analysis for reacted pure gypsum sample.*

Figures 22 and 24 display the pure gypsum sample before and after experimentation. The unreacted sample has much larger grains that are more compact compared to the reacted sample. The reacted sample is more fibrous and qualitatively similar the gypsum displayed in the images of the Sample 9 polished thin sections displayed in Chapter 2. The reacted gypsum in Fig. 24 is similar to the expected morphology of gypsum. The purchased sample was indicated formulaically to be gypsum, however the unreacted gypsum in Fig. 22 is more like the expected morphology of anhydrite, the anhydrous version of gypsum ($CaSO_4$). It is hypothesized that anhydrite was sent

by mistake, and the addition of brine hydrated the sample allowing individual grains to disperse from the original conglomerate grains and appear as gypsum.

Figures 23 and 25 display the electron dispersive spectroscopy (EDS) analysis of the indicated spots in the unreacted and reacted gypsum samples respectively. Both are indicative of the expected spectra for gypsum. However, the unreacted spectra suggests much lower levels of oxygen present in than the reacted spectra, which supports the hypothesis that anhydrite was sent by mistake. Unfortunately, the expected spectra of anhydrite and gypsum are very similar, and EDS analysis is not sufficient for quantitative mineral composition, therefore further analysis is required to confirm or deny the hypothesis of accidental anhydrite (Welton, 2003). The trace amounts of boron and aluminum are present in the spectra are assumed to be error, as the SEM was run in variable pressure mode which is known to cause some error in EDS analysis.

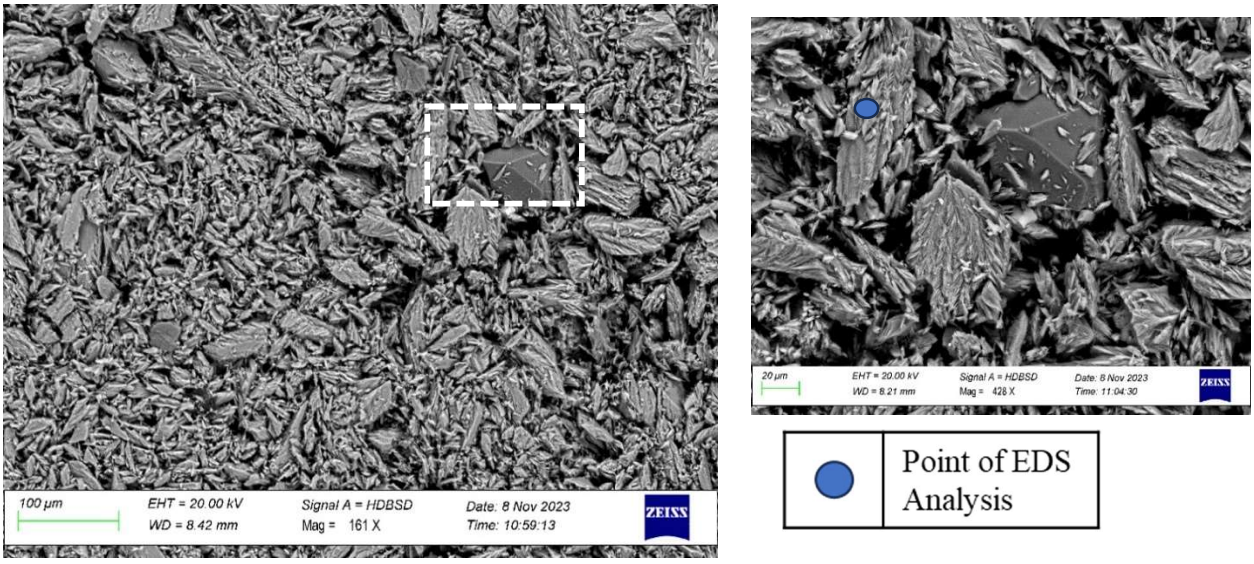


*Figure 26. Unreacted Sample 9 grains at two resolutions. The dotted line represents the region of interest for the right image which displays a quartz grain surrounded by fibrous gypsum.*

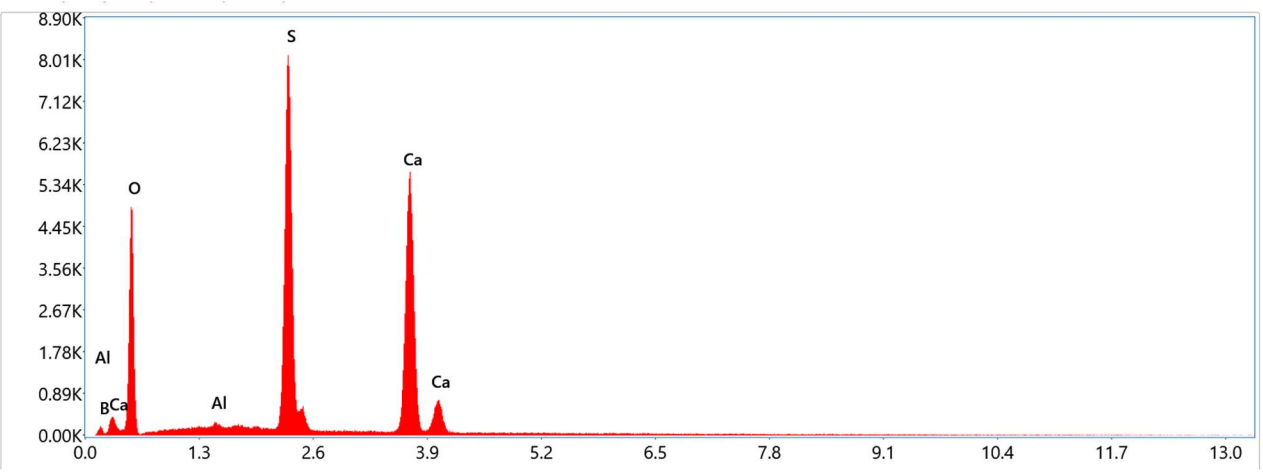


*Figure 27. EDS spot analysis for unreacted Sample 9.*

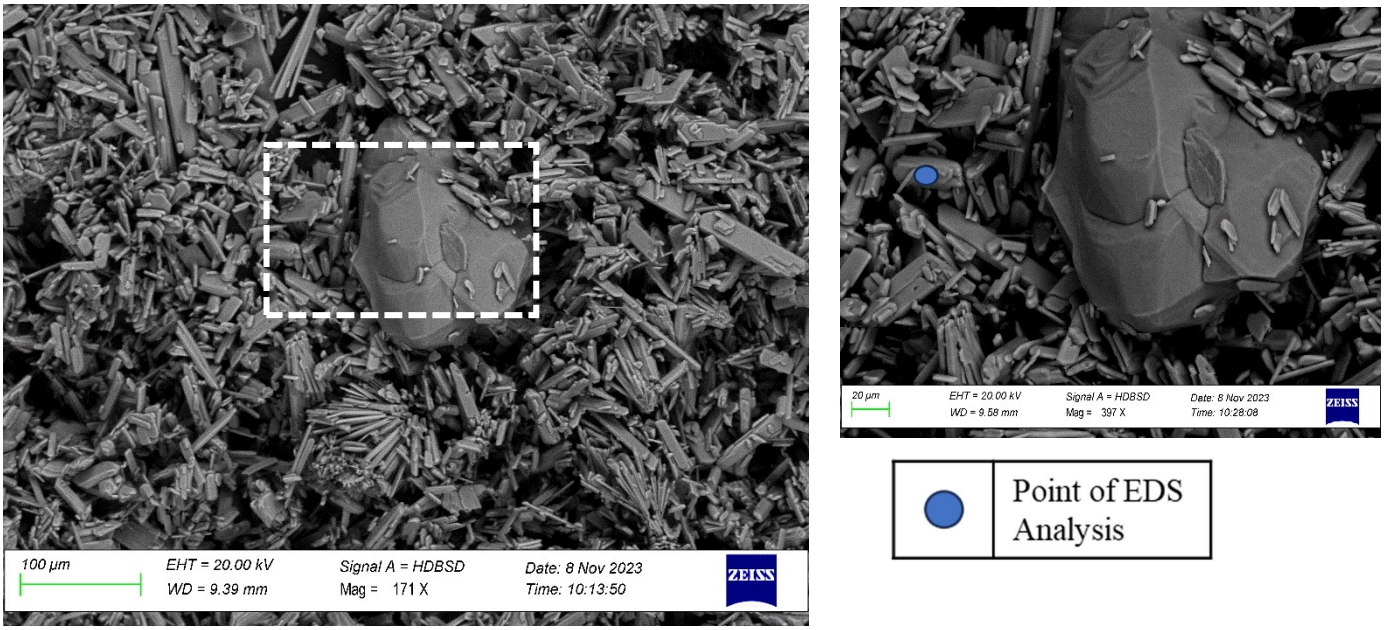


*Figure 28. Reacted Sample 9 at two separate resolutions. The dotted line represents the region of interest for the right image where a quartz grain surrounded by fibrous gypsum is displayed.*

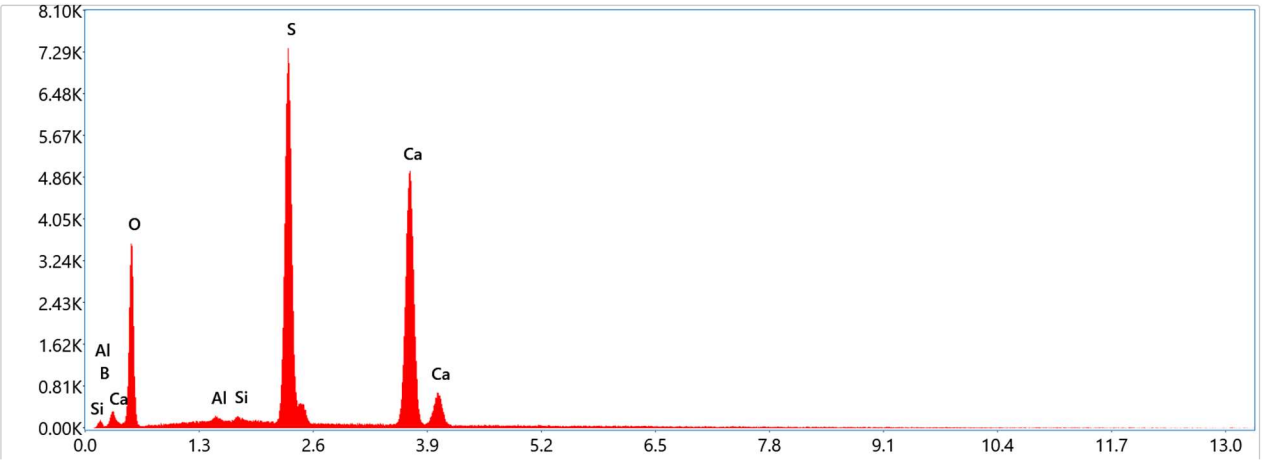


*Figure 29. EDS spot analysis of reacted Sample 9.*

Figures 26 and 28 display Sample 9 before and after reaction at different resolutions. In both sets of images, a quartz grain surrounded by fibrous gypsum grains are shown. Before reaction, the gypsum grains are more densely packed together with a rough texture. After the reaction, the gypsum grains are less densely packed and have a smoother, more uniform texture.

Figures 27 and 29 display the EDS analysis results for unreacted and unreacted Sample 9, which indicates that the gypsum in the sample remains the same. The spots chosen for this analysis were both hypothesized to be gypsum grains.

Figures 24 and 28 display similarities in the structure of the reacted synthetic pure gypsum and the reacted gypsum found in Sample 9. With the addition of $CO_2$ and brine, the gypsum in these samples became more uniformly fibrous and less densely compacted from their respective original state.

### 3.4 Conclusion

In this work, Parr batch reactor experiments were conducted to determine whether gypsum will dissolve in the presence of $CO_2$ saturated brine in conditions relevant to geologic carbon

sequestration. The experiment conditions were based upon the Cassville, GA stratigraphic test well site. Week-long experiments were run for both pure gypsum and the gypsum-rich Sample 9 from the Cassville, GA well. SEM imaging was utilized to display the qualitative differences between the reacted and unreacted samples.

The experiments suggest that although some dissolution occurred, over 99.9% of the gypsum remained solid in both cases. This suggests that gypsum is not likely to dissolve significantly at conditions relevant to GCS in the context of $CO_2$ at this time scale. This supports the modeling results from Chapter 2 that suggest gypsum will remain stable throughout the injection period of GCS. The SEM images of the pre and post experiment samples display differences in the morphology of gypsum. However, it is worthwhile to note the qualitative similarities in the gypsum grains observed in both reacted samples. In continuation of this work, each sample could undergo XRD analysis to confirm the mineralogy of the reacted and unreacted samples. Additionally, reactive transport modeling of these experiments could help validate the chosen reaction rate chosen for the simulations in Chapter 2.

# Chapter 4. Contributions to new knowledge

## 4.3 The nature of gypsum in acidic, high-pressure environments

In the first study, injection of $CO_2$ into a gypsum-rich formation in Cassville, GA was considered. The micro-continuum scale reactive transport code Crunchflow was used to simulate the geochemical reactions that could occur with the addition of $CO_2$ to the formation and the subsequent effects on the $CO_2$ and formation itself. There is a lack of published studies concerning the nature of gypsum in the conditions relevant to GCS: acidic, high-pressure, high-temperature environments. The results from this study suggest that gypsum will remain stable in these conditions, meaning it will neither dissolve nor precipitate significantly.

The results from the second experimental study support the findings from the first. Two separate batch experiments were conducted: one with pure gypsum and one using Sample 9 from Cassville, GA. These samples were subjected to the formation pressure and temperature in the presence of brine and $CO_2$. Although some gypsum dissolution occurred as displayed by the amount of calcium ions in solution, as a whole the gypsum remained stable in both cases.

## 4.4 Unlikelihood of mineral trapping during injection of $CO_2$ in gypsum-rich reservoirs

Precipitation of calcite and other carbonate minerals may occur in storage reservoirs, permanently trapping $CO_2$ as new mineral phases. Simulations in this work sought to predict whether the conditions of this reservoir were such to promote such carbonate mineral precipitation. The simulation results suggest that $CO_2$ will not transform to calcite via mineral precipitation reactions if stored in gypsum dominated deep saline aquifers. Although existing as free $CO_2$ and dissolved $CO_2$ are considered “less permanent” forms of sequestration than mineral trapping, the amount of $CO_2$ that can be stored is not limited by a decrease in reservoir permeability that may

result from associated mineral trapping. This could make a gypsum-rich site more economically favorable from the standpoint that injectivity will be maintained during injection. However, increased permeability may also promote further migration of the CO2 plume away from the well and require additional monitoring.

### 4.5 Fate of injected $CO_2$ at potential Cassville, GA site

The study in its entirety sought to predict the fate of $CO_2$ if were injected into the gypsum-rich layer of the Cassville, GA well. The simulated results from the reactive transport models suggest that mineral trapping via calcite precipitation of the injected $CO_2$ is unlikely to occur within the injection period. The potential for mineral trapping in the post-injection period was not evaluated. The simulated injection of $CO_2$ causes a drop in pH affecting the entirety of the 38-meter model; however, the pH is buffered spatially until dolomite is consumed. This suggests a more extreme anticipated extent of mineral dissolution during injection than reality, as this simulated a $CO_2$ acidified brine whereas in actuality, there will be a complex phase flow two phase flow system which could reduce the extent of reaction.

It is worthwhile to note that this layer of the aquifer is an anomaly from the rest which is comprised primarily of dolostones. To accurately predict the fate of $CO_2$ if it were to be injected into this well at various depths, a separate analysis must occur.

## References

A RAPID RESPONSE ASSESSMENT SPREADING LIKE WILDFIRE THE RISING THREAT OF EXTRAORDINARY LANDSCAPE FIRES. (2022). http://www.un.org/Depts/

Azdarpour, A., Asadullah, M., Junin, R., Manan, M., Hamidi, H., & Mohammadian, E. (2014). Direct carbonation of red gypsum to produce solid carbonates. *Fuel Processing Technology*, *126*, 429–434. https://doi.org/10.1016/j.fuproc.2014.05.028

Bachu, S. (2000). Sequestration of CO2 in geological media: criteria and approach for site selection in response to climate change. *Energy Conversion and Management*, *41*(9), 953–970. https://doi.org/10.1016/S0196-8904(99)00149-1

Baniak, G. M., Gingras, M. K., & Pemberton, S. G. (2013). Reservoir characterization of burrow-associated dolomites in the Upper Devonian Wabamun Group, Pine Creek gas field, central Alberta, Canada. *Marine and Petroleum Geology*, *48*, 275–292. https://doi.org/10.1016/j.marpetgeo.2013.08.020

Croft, M. G. (n.d.). *Geology and Ground-Water Resources of Bartow County Georgia Prepared in cooperation with the Georgia Department of Mines, Mining, and Geology UNITED STATES GOVERNMENT PRINTING OFFICE, WASHINGTON ; 1963*.

Cucchi, F., Franceschini, G., & Zini, L. (2008). Hydrogeochemical investigations and groundwater provinces of the Friuli Venezia Giulia Plain aquifers, northeastern Italy. *Environmental Geology*, *55*(5), 985–999. https://doi.org/10.1007/s00254-007-1048-4

Dai, Z., Xu, L., Xiao, T., McPherson, B., Zhang, X., Zheng, L., Dong, S., Yang, Z., Soltanian, M. R., Yang, C., Ampomah, W., Jia, W., Yin, S., Xu, T., Bacon, D., & Viswanathan, H. (2020).

Reactive chemical transport simulations of geologic carbon sequestration: Methods and applications. *Earth-Science Reviews*, *208*, 103265. https://doi.org/10.1016/J.EARSCIREV.2020.103265

Dávila, G., García-Rios, M., Soler, J. M., & Cama, J. (n.d.). *Modeling dolomite-brine interaction in the context of geological CO 2 sequestration*.

Ebrahimi, P., & Vilcáez, J. (2018). Effect of brine salinity and guar gum on the transport of barium through dolomite rocks: Implications for unconventional oil and gas wastewater disposal. *Journal of Environmental Management*, *214*, 370–378. https://doi.org/10.1016/j.jenvman.2018.03.008

Garcia-Rios, M., Cama, J., Luquot, L., & Soler, J. M. (2014). Interaction between CO2-rich sulfate solutions and carbonate reservoir rocks from atmospheric to supercritical CO2 conditions: Experiments and modeling. *Chemical Geology*, *383*, 107–122. https://doi.org/10.1016/j.chemgeo.2014.06.004

Gleeson, J., Woessner, D. E., & Jordan Jr, C. F. (1993). *NMR Imaging of Pore Structures in Limestones*. http://onepetro.org/FE/article-pdf/8/02/123/2608719/spe-20493-pa.pdf/1

Han, B., Xie, S. Y., & Shao, J. F. (2016). Experimental Investigation on Mechanical Behavior and Permeability Evolution of a Porous Limestone Under Compression. *Rock Mechanics and Rock Engineering*, *49*(9), 3425–3435. https://doi.org/10.1007/s00603-016-1000-6

Hao, Y., Smith, M., Sholokhova, Y., & Carroll, S. (2013). CO2-induced dissolution of low permeability carbonates. Part II: Numerical modeling of experiments. *Advances in Water Resources*, *62*, 388–408. https://doi.org/10.1016/j.advwatres.2013.09.009

Harris, D. C. (2010). *Quantitative chemical analysis*. Macmillan.

Kang, Q., Lichtner, P. C., Viswanathan, H. S., & Abdel-Fattah, A. I. (2010). Pore scale modeling of reactive transport involved in geologic CO2 sequestration. *Transport in Porous Media*, *82*(1), 197–213. https://doi.org/10.1007/s11242-009-9443-9

Kang, Q., Lichtner, P. C., & Zhang, D. (2006). Lattice Boltzmann pore-scale model for multicomponent reactive transport in porous media. *Journal of Geophysical Research: Solid Earth*, *111*(5). https://doi.org/10.1029/2005JB003951

Klimchouk, A. (n.d.). *Chapter 1.2 THE DISSOLUTION AND CONVERSION OF GYPSUM AND ANHYDRITE Alexander Klimchouk*.

Klimchouk, A., Cucchi, F., Calaforra, J. M., Aksem, S., Finocchiaro, F., & Forti, P. (1996). Chapter 1.3 DISSOLUTION OF GYPSUM FROM FIELD OBSERVATIONS. In *Int. J. Speleol* (Vol. 25, Issue 4).

Kong, L., Ostadhassan, M., Li, C., & Tamimi, N. (2018). Pore characterization of 3D-printed gypsum rocks: a comprehensive approach. *Journal of Materials Science*, *53*(7), 5063–5078. https://doi.org/10.1007/s10853-017-1953-1

Labus, K., & Bujok, P. (2011). CO2 mineral sequestration mechanisms and capacity of saline aquifers of the Upper Silesian Coal Basin (Central Europe) - Modeling and experimental verification. *Energy*, *36*(8), 4974–4982. https://doi.org/10.1016/j.energy.2011.05.042

Lal, R. (2008). Carbon sequestration. In *Philosophical Transactions of the Royal Society B: Biological Sciences* (Vol. 363, Issue 1492, pp. 815–830). Royal Society. https://doi.org/10.1098/rstb.2007.2185

Lee, M. gyu, Jang, Y. N., Ryu, K. won, Kim, W., & Bang, J. H. (2012). Mineral carbonation of flue gas desulfurization gypsum for CO2 sequestration. *Energy*, *47*(1), 370–377. https://doi.org/10.1016/j.energy.2012.09.009

Lucia, F. J. (n.d.). *Origin and petrophysics of dolostone pore space*. https://www.lyellcollection.org

MacMinn, C. W., & Juanes, R. (2009). A mathematical model of the footprint of the CO2 plume during and after injection in deep saline aquifer systems. *Energy Procedia*, *1*(1), 3429–3436. https://doi.org/10.1016/j.egypro.2009.02.133

Rendel, P. M., Gavrieli, I., Wolff-Boenisch, D., & Ganor, J. (2016). Gypsum solubility under pressure conditions relevant to CO2 geological storage. *International Journal of Greenhouse Gas Control*, *55*, 15–22. https://doi.org/10.1016/j.ijggc.2016.10.017

Rosenbauer, R. J., Koksalan, T., & Palandri, J. L. (2005). Experimental investigation of CO2–brine–rock interactions at elevated temperature and pressure: Implications for CO2 sequestration in deep-saline aquifers. *Fuel Processing Technology*, *86*(14–15), 1581–1597. https://doi.org/10.1016/J.FUPROC.2005.01.011

Smith, M. M., Hao, Y., & Carroll, S. A. (2017a). Development and calibration of a reactive transport model for carbonate reservoir porosity and permeability changes based on CO2 core-flood experiments. *International Journal of Greenhouse Gas Control*, *57*, 73–88. https://doi.org/10.1016/j.ijggc.2016.12.004

Smith, M. M., Hao, Y., & Carroll, S. A. (2017b). Development and calibration of a reactive transport model for carbonate reservoir porosity and permeability changes based on CO2

core-flood experiments. *International Journal of Greenhouse Gas Control*, *57*, 73–88. https://doi.org/10.1016/j.ijggc.2016.12.004

Smith, M. M., Sholokhova, Y., Hao, Y., & Carroll, S. A. (2013). CO2-induced dissolution of low permeability carbonates. Part I: Characterization and experiments. *Advances in Water Resources*, *62*, 370–387. https://doi.org/10.1016/j.advwatres.2013.09.008

Song, K., Jang, Y. N., Kim, W., Lee, M. G., Shin, D., Bang, J. H., Jeon, C. W., & Chae, S. C. (2014). Factors affecting the precipitation of pure calcium carbonate during the direct aqueous carbonation of flue gas desulfurization gypsum. *Energy*, *65*, 527–532. https://doi.org/10.1016/j.energy.2013.11.008

Tutolo, B. M., Luhmann, A. J., Kong, X. Z., Saar, M. O., & Seyfried, W. E. (2014). Experimental observation of permeability changes in dolomite at CO 2 sequestration conditions. *Environmental Science and Technology*, *48*(4), 2445–2452. https://doi.org/10.1021/es4036946

Voorn, M., Exner, U., Barnhoorn, A., Baud, P., & Reuschlé, T. (2015). Porosity, permeability and 3D fracture network characterisation of dolomite reservoir rock samples. *Journal of Petroleum Science and Engineering*, *127*, 270–285. https://doi.org/10.1016/j.petrol.2014.12.019

Vose, R. S., Easterling, D. R., Kunkel, K. E., LeGrande, A. N., & Wehner, M. F. (2017). *Ch. 6: Temperature Changes in the United States. Climate Science Special Report: Fourth National Climate Assessment, Volume I*. https://doi.org/10.7930/J0N29V45

Warren, J. (n.d.). Dolomite: occurrence, evolution and economically important associations. In *Earth-Science Reviews* (Vol. 52). www.elsevier.comrlocaterearscirev

Xie, M., Mayer, K. U., Claret, F., Alt-Epping, P., Jacques, D., Steefel, C., Chiaberge, C., & Simunek, J. (2015). Implementation and evaluation of permeability-porosity and tortuosity-porosity relationships linked to mineral dissolution-precipitation. *Computational Geosciences*, *19*(3), 655–671. https://doi.org/10.1007/s10596-014-9458-3

Yang, C., Dai, Z., Romanak, K. D., Hovorka, S. D., & Treviño, R. H. (2014). Inverse modeling of water-rock-CO2 batch experiments: Potential impacts on groundwater resources at carbon sequestration sites. *Environmental Science and Technology*, *48*(5), 2798–2806. https://doi.org/10.1021/es4041368

Yu, L., Daniels, L. M., Mulders, J. J. P. A., Saldi, G. D., Harrison, A. L., Liu, L., & Oelkers, E. H. (2019). An experimental study of gypsum dissolution coupled to CaCO3 precipitation and its application to carbon storage. *Chemical Geology*, *525*, 447–461. https://doi.org/10.1016/j.chemgeo.2019.08.005

Zhang, L., Soong, Y., & Dilmore, R. M. (2017). Numerical investigation of Lower Tuscaloosa Sandstone and Selma Chalk caprock under geological CO2 sequestration conditions: mineral precipitation and permeability evolution. *Greenhouse Gases: Science and Technology*, *7*(6), 988–1007. https://doi.org/10.1002/ghg.1703

Zhang, Q., Deng, H., Dong, Y., Molins, S., Li, X., & Steefel, C. (2022). Investigation of Coupled Processes in Fractures and the Bordering Matrix via a Micro-Continuum Reactive Transport Model. *Water Resources Research*, *58*(2). https://doi.org/10.1029/2021WR030578

Azdarpour, A., Asadullah, M., Junin, R., Manan, M., Hamidi, H., Mohammadian, E., 2014. Direct carbonation of red gypsum to produce solid carbonates. Fuel Process. Technol. 126, 429–434.